

2011

Modeling Nano-Particle Migration in Pipe Flow through Eulerian-Lagrangian Approach

Kai Jin

Lehigh University

Follow this and additional works at: <http://preserve.lehigh.edu/etd>

Recommended Citation

Jin, Kai, "Modeling Nano-Particle Migration in Pipe Flow through Eulerian-Lagrangian Approach" (2011). *Theses and Dissertations*. Paper 1253.

This Thesis is brought to you for free and open access by Lehigh Preserve. It has been accepted for inclusion in Theses and Dissertations by an authorized administrator of Lehigh Preserve. For more information, please contact preserve@lehigh.edu.

Modeling Nano-Particle Migration in Pipe Flow through Eulerian-Lagrangian Approach

By

Kai Jin

A Thesis

Presented to the Graduate and Research Committee

of Lehigh University

in Candidacy for the Degree of

Master of Science

In

Mechanical Engineering

Lehigh University

July 2011

Copyright© 2011

Kai Jin

All rights reserved

Thesis is accepted and approved in partial fulfillment of the requirements for the Master of Science in Mechanical Engineering

Modeling Nano-Particle Migration in Pipe Flow through Eulerian-Lagrangian Approach

Kai Jin

Date Approved

Dr. Sudhakar Neti
Co-Advisor

Dr. Alparslan Oztekin
Co-Advisor

Dr. Gary Harlow
Department Chair Person

ACKNOWLEDGEMENTS

I would like to take this time to express my sincere gratitude and appreciation to everyone who contributed to this research. Firstly, I'd like to thank both my advisors, Dr. Sudhakar Neti and Dr. Alparslan Oztekin, for their extensive guidance and assistance during the past two years. It would have been impossible for me to finish this research without their continuous support and encouragement.

Thank you to Dr. Yaling Liu, professor in Mechanical Engineering and Mechanics for his suggestions on particle tracking and two-phase flow modeling. Thank you to Ali F. Elmozughi for discussing research with me, helping in Ansys Fluent and his encouragement. I also would like to thank Dr. Yijun Yang for his suggestions on two-phase flow modeling. Thanks to my friend Ben Rosenzweig and Yuvraj Singh for their help in my thesis writing. I'd like to thank all my colleagues and friends at Lehigh University, who provided continuous encouragement and support during my study at Lehigh.

TABLE OF CONTENTS#

| | |
|---|-----|
| ACKNOWLEDGEMENTS | iv |
| TABLE OF CONTENTS | v |
| LIST OF FIGURES | vii |
| LIST OF TABLES | ix |
| ABSTRACT | 1 |
| Chapter 1. Introduction | 2 |
| Chapter 2. Literature Review | 4 |
| Chapter 3. Flow Geometry - Mesh Configuration | 9 |
| 3.1. Geometry of Computational Domain | 9 |
| 3.2. Mesh Configuration..... | 10 |
| 3.3. Spatial Convergence Test..... | 12 |
| 3.4. Base fluid, Nanoparticles and Pipe..... | 13 |
| Chapter 4. Modeling and Results of Laminar Flow | 15 |
| 4.1. Laminar Flow(Single Phase) | 15 |
| 4.2. Particle Tracking in Laminar Flow by Eulerian-Lagrangian Method | 20 |
| 4.2.1. Two-way Coupling..... | 20 |
| 4.2.2. Equations of Motion for Particles..... | 22 |
| 4.2.3. Integration of Particle Motion Equation..... | 23 |
| 4.2.4. Modeling the Drag Coefficients | 24 |
| 4.2.5. Momentum and Mass Exchanges | 27 |
| 4.2.6. Brownian Motion..... | 28 |
| 4.2.7. Simulation Configurations..... | 29 |
| 4.2.8. Results and Discussion for Laminar Eulerian-Lagrangian Approach | 30 |
| Chapter 5. Modeling and Results of Turbulent Pipe Flow | 39 |
| 5.1. Turbulent Flow(Single Phase)..... | 39 |
| 5.2. Reynolds-averaged Navier-Stokes (RANS) Equations and k- ϵ Model | 41 |
| 5.3. k- ϵ Model..... | 43 |
| 5.4. Stochastic Tracking of Particles - Random Walk Model | 45 |
| 5.4.1. Integration Time | 45 |
| 5.4.2. Discrete Random Walk Model | 46 |
| 5.5. Simulation Configurations..... | 48 |

| | |
|--|----|
| 5.6. Results and Discussion of Particle Migration in Turbulent Flow under k- ϵ model..... | 51 |
| Chapter 6. Conclusions | 59 |
| Chapter 7. Future Research | 61 |
| BIBLIOGRAPHY | 62 |
| VITA | 66 |

LIST OF FIGURES

| | |
|---|----|
| Figure 1. Geometry of Computational Cell | 9 |
| Figure 2. Part of the Mesh of Computational Domain..... | 10 |
| Figure 3. Mesh Sensitivity Check: Comparison of Outlet Axis Velocity..... | 12 |
| Figure 4. Mesh Sensitivity Check: Comparison of Outlet Axis Velocity..... | 13 |
| Figure 5. Flow Chart of Pressure-based Algorithm Used in Fluid Solver..... | 18 |
| Figure 6. Comparison between Analytical Solution and Simulation Results: Axial Velocity Profile of Fully Developed Laminar Flow (Dimensionless) | 19 |
| Figure 7. Dimensionless Velocity Profile of Fluid at Different Cross-sections ($x=0.0$ m, $x=0.2$ m, $x=0.4$ m, $x=0.6$ m and $x=0.8$ m) in Laminar Pipe Flow with Particles Injection of 1% volume fraction, exclude Brownian Force. | 30 |
| Figure 8. Comparison of Velocity Profiles for Both Cases (with and without Particles Injections) at Different Cross-sections ($x=0.0$ m, $x=0.4$ m & $x=0.8$ m), Laminar Flow without Brownian Force..... | 31 |
| Figure 9. Enlarged Figure, Showing the Intersection of the Velocity Profiles of Flow with and without Particle Injections at $x=0.4$ m and $x=0.8$ m..... | 32 |
| Figure 10. Trajectories are colored by velocity magnitude. | 34 |
| Figure 11. Histogram of Particle Locations Histogram of Particle Locations at Varies Cross sections for Laminar Flow with Plug Flow Inlet..... | 35 |
| Figure 12. Particle trajectories for fully developed laminar flow | 36 |
| Figure 13. Histogram of Particle Locations at Varies Cross Sections for Laminar Pipe Flow with Fully Developed Parabolic Inlet..... | 37 |
| Figure 14. Turbulent Velocity Profile for Fully Developed Flow in a Smooth Pipe..... | 40 |
| Figure 15. Boundary Conditions of Axial Velocity, k and ϵ at Pipe Inlet..... | 50 |
| Figure 16. Histograms of Particle Locations at Various Cross Sections for Case 2..... | 53 |

| | |
|---|----|
| Figure 17. Histograms of Particle Locations at Various Cross Sections for Case 4..... | 54 |
| Figure 18. Histograms of Particle Locations at Various Cross Sections for Case 7..... | 54 |
| Figure 19. Particle Trajectories Colored by Particle Velocity | 55 |
| Figure 20. Turbulence Intensity vs r/R for 1% Particle Volume Fraction..... | 56 |
| Figure 21. Turbulence Dissipation rate at Outlet vs Dimensionless Radius..... | 57 |

LIST OF TABLES

| | |
|---|----|
| Table 1. Mesh Configuration in Radius and Axis Directions | 12 |
| Table 2. Properties of Water | 14 |
| Table 3. Property of Nanoparticles (Carbon)..... | 14 |
| Table 4. Property of Pipe Wall | 14 |
| Table 5. Drag-Reynolds-Number Relationship | 25 |
| Table 6. B.C. for Turbulence Cases of Varies Particles Concentrations | 48 |
| Table 7. Nanoparticles Effect on Friction Coefficient and Moody Coefficient Factor | 51 |

ABSTRACT

Numerical simulations of fluid and nanoparticles (nanofluids) two-phase flows are conducted using finite volume method. Eulerian-Lagrangian approach is employed to study the nature of both laminar and turbulent flow fields of fluid phase as well as kinematic and dynamic of dispersed nanoparticles. Effects of two-way interaction between fluid and particles and the Saffman lift force are included. The effects of nanoparticle size and volume fraction of nanoparticles on the laminar and turbulent flow field are investigated. Numerical simulations conducted for the range of the particle size from 100 nm to 5 μm and the range of particle concentrations from 1% to 10% in volume. Our results indicate that in developing laminar flow, nanoparticles have tendency to migrate toward the center, while in fully developed laminar flow nanoparticles follow streamlines and remain parallel for Reynolds number of 507. Present work also predicts that nanoparticles have tendency to migrate to a region close to the wall ($0.65 < r/R < 0.95$) in turbulent flow for Reynolds number of about 20,000. The presence of nanoparticles increases the turbulence intensity slightly, but a significant increase of turbulence dissipation rate is observed in some region. The turbulence intensity is not very sensitive to particle size or particle concentrations while turbulence dissipation rate increases slightly with increasing particle concentration. Nanofluid can potentially be used as an advanced heat transfer fluid. The influence of nanoparticles on the turbulence intensity and turbulence dissipation rate could alter the heat transfer coefficients in these systems.

Chapter 1. Introduction

“Nanofluids”, which are engineered suspensions of nanoparticles in liquids, have been developed and studied during the last decades. To determine the physical properties of this kind of fluid, a wide variety of nanofluids have been made and their properties were evaluated. Worldwide many investigators have done numerous experiments to study the thermophysical properties of nanofluids, with particular emphasis on the measurements of their effective thermal conductivity and viscosity. Scientists and companies are interested in their potential to enhance the effective heat transfer rate in heat exchanger and other engineering systems, and in the mean time reducing the sedimentation, clogging and erosion issues that generated by solid-liquid mixtures with larger particles.

In order to understand how the nanoparticles influence the thermal physical properties of nanoflow, the kinematics and dynamics of the nanoparticles are investigated. Considering pipe flow, the most frequently used configurations in practice, as an example, if the nanoparticles can increase the radial velocity/radial fluctuation of the flow, it will help with mixing the fluid in the pipe and finally increase the heat transfer from the wall of pipe to fluid. After the solution of the two-phase flow field is determined, proper thermal boundary conditions could be added and the heat transfer property of nanofluid can be studied. Hence, for our purposes, two-phase fluid which contains water as the first phase and carbon as the second phase will be modeled.

The commercial software Ansys Fluent is used to model nanofluids travelling in a pipe with diameter of 2 cm. The particles selected are spherical carbon with diameter from 100 nm to 500 nm and the density of the particles is 2000 kg/m^3 . During the

simulation the nanoparticles are maintained at volume fraction from 1% to 10%. To study the affect of injection position and injection method, the particles are injected at the inlet of the pipe by both uniform injection and non-uniform injection.

Both laminar and turbulent flows with Reynolds numbers up to 2×10^4 are examined. In the laminar case, the standard Navier Stokes equations are solved by the finite volume method provided by Fluent. Regarding the turbulent case, the steady state Reynolds-averaged Navier Stokes (RANS) model is employed. In the present study, the Eulerian-Lagrangian method is applied. Eulerian-Lagrangian method is used to track the trajectory of an individual stream of nanoparticles, to illustrate whether the particles are moving toward the wall or moving away from the wall. During the modeling, the interaction between the fluid phase (water) and the solid phase (carbon particles) are considered and involved by using two-way coupling, which means the fluid can affect the particle motion by drag, and in the other hand the particles can exchange momentum and mass with the continuous fluid. The dispersion of particles due to turbulence in the fluid phase was also taken into account by using the stochastic tracking model.

The subsequent chapters will be arranged as follows: Chapter Two will give a general introduction of nanofluids and brightly go over past studies related to nanofluids; Chapter Three will discuss the modeling geometry, mesh and the property of the fluid and particles used in the simulation; Chapter Four will cover the theory and the detailed method used in modeling laminar case; Chapter Five will discuss the theory of turbulent flow and tracking particles in turbulent flow, then the modeling results will be discussed; Chapter Six will go over the conclusions; and Chapter Seven will discuss future work.

Chapter 2. Literature Review

The idea of adding highly conductive particles into fluid to enhance the thermal conductivity of base fluid can trace back to more than 100 years ago. In the past half century, scientists have developed a number of theoretical models which can predict the effective thermal conductivity of these mixtures. Among those models, the most popular ones are the Maxwell¹ model (Eqn. 1), and Hamilton Crosser model². In Maxwell model, k is the thermal conductivity of nanofluid, k_f is the thermal conductivity of the base fluid, ϕ is the particle volumetric fraction and k_p is the thermal conductivity of added particles

$$\frac{k}{k_f} = \frac{k_p + 2k_f + 2\phi(k_p - k_f)}{k_p + 2k_f - \phi(k_p - k_f)} \quad (1)$$

To predict the effective thermal conductivity of suspension fluid, Maxwell and the Hamilton Crosser model both include the effect of volume fraction, the particle shape, and the thermal conductivity ratio between the suspended particles and base fluid. However, they fail to consider the effect of particle size and the fluid temperature. At that time, due to the limitation of manufacturing technology, particle sizes were limited to micrometer or millimeters. Because the size of dispersed particles is relatively large, the mixture fluid often has the problem of clogging, sedimentation, and abrasion. All these issues make it hard to realize the concept in practice.

In the last two decades, the rapid development of modern nanotechnology enabled the production of particles and tubes with average sizes below 100 nm. Compared with conventional bulk particles, these nanoparticles show dramatic change in their mechanical, optical, electrical, magnetic, and thermal properties. Specially, some of

them, even in high volume fraction, do not have the problems of clogging and sedimentation. Noticing the great advantage of nanoparticles and taking advantage of the advanced manufacturing techniques, Choi³ and his group in Argonne National Laboratory first started to add nano-sized metallic particles with high thermal conductivities to fluid and began to investigate the thermal conductivity of such fluid. It's also from that time, they named the liquids with suspensions of nanoparticles "nanofluid".

According to studies by Choi in 1995⁴ and 2001⁵, the Maxwell and the Hamilton Crosser models do not accurately predict the results of the thermal conductivity of a nanofluid. His research group employed a transient hot wire method to study the nanofluid with multiwall carbon nanotubes dispersed in oil. After they calculated the thermal conductivity of this nanofluid, they found that the results were of one order magnitude greater than the Maxwell model had predicted. In contrast with the Maxwell model, their group found that there was not a linear relationship between the increase in thermal conductivity and the volume fraction of nanoparticles dispersed in the base fluid.

Similar to Choi's group, other groups reported great enhancement of thermal conductivity of the nanofluid. H. Chen et al⁶ found their aqueous suspension of titanate nanotubes had aspect ratio about 10, having much higher thermal conductivity enhancement than that predicted by Hamilton-Cross model. H. U. Kang et al⁷ measured the thermal conductivities of nanofluid containing ultra-dispersed diamond (UDD), silver, and silica nanoparticles by using a transient hot-wire method, and their experiments results showed a great increase of thermal conductivity (in the case of 1% UDD in Ethylene glycol, the thermal conductivity was enhanced about 70%). M. Chopkar⁸ et al

made nanofluid with a low concentration of nanocrystalline metallic particles ($\text{Al}_{70}\text{Cu}_{30}$) dispersed in ethylene glycol and observed a “significantly greater (1.2–2 times)” enhancement of thermal conductivity than that of the base fluid, as well as that predicted by the existing models. The corresponding studies show great promise in the thermal conductivity capabilities of nanofluids.

To explain the dramatic enhancement of thermal conductivity of nanofluid compared with the base fluid, scientists proposed several hypotheses: 1) nanoparticles may form clusters or agglomerates within the nanofluid, hence most heat is transferred along such percolating clusters or agglomerates;⁹ 2) the Brownian motion of nanoparticles agitates the fluid, thus creating a microconvection effect that increases energy transport;¹⁰ 3) basefluid molecules encompass the dispersed nanoparticles and formed a highly ordered high thermal-conductivity, thus augmenting the effective volumetric fraction of the particles and increased the thermal conductivity of nanofluids.¹¹

In order to better understand the properties of nanofluids, Buongiorno¹² launched an international nanofluid property benchmark exercise (INPBE) in 2007. 34 research centers around the world participated in this program and measured the properties of some nanofluids. Their results show the thermal conductivity enhancement of the tested nanofluids increased with increasing particle loading, particle aspect ratio, and decreasing base fluid thermal conductivity, which is consistent with the effective medium theory for well-dispersed particles that is developed by Nan et al¹³. Nan’s model, as described in Eqn, 2, includes the effects of particle geometry and finite interfacial resistance.

$$\frac{k}{k_f} = \frac{3 + \phi [2\beta_{11}(1 - L_{11}) + \beta_{33}(1 - L_{33})]}{3 - \phi(2\beta_{11}L_{11} + \beta_{33}L_{33})} \quad (2)$$

Where for particles shaped as prolate ellipsoids with principal axes $a_{11}=a_{22}<a_{33}$

$$L_{11} = \frac{p^2}{2(p^2 - 1)} - \frac{p^2}{2(p^2 - 1)^{3/2}} \cosh^{-1} p$$

$$L_{33} = 1 - 2L_{11}, \quad p = a_{33} / a_{11},$$

$$\beta_{ii} = \frac{k_{ii}^c - k_f}{k_f + L_{ii}(k_{ii}^c - k_f)}, \quad k_{ii}^c = \frac{k_p}{1 + \gamma L_{ii} k_p / k_f}$$

$$\gamma = \frac{(2 + 1/p) R_{bd} k_f}{0.5 a_{11}}$$

These results also suggest that no anomalous enhancement of thermal conductivity was observed in the nanofluids test by INPBE.

The variety of the corresponding studies indicates that the flow and nanoparticles behavior may have imposed some important effect on the heat transfer property of nanofluids. However, most of these experimental results provide limited information of the mechanisms by which these enhancements are obtained, such as factors like particle clustering, migration and interactions with the walls, etc. influence on the behavior of nanofluids.

There are also some other research groups who put their emphasis on the flow behavior of nanofluids. Ding and Wen ,2004¹⁴, studied particle migration in pressure-driven laminar pipe flows, and their model included particle migrations caused by shear and viscosity gradient, as well as self-diffusion due to the Brownian motion. They reported that “particle concentration in the wall region can be much lower than that in the

central core region.” After that, M Giraldo et al¹⁵ employed a boundary integral formulation approach and simulated a flow containing about 1.05% volume fraction Al_2O_3 with diameter of 30 nm in water in the vicinity of a plane wall in a rectangular region with 1.5 μm high, 10 μm long. They included effects from Brownian motion, Van der Waals attraction, electrostatic short range repulsion forces and buoyancy, and observing high cross flow velocities in the boundary layer and a zone with 17% higher concentration 0.3 μm away from the wall.

Hence, understanding of the flow behavior, particles behavior near wall, and particle migration in nanofluids is important for the future utilization of nanofluids as potential heat transfer media. The author did some simulations by using Eulerian-Lagrangian model to study the behavior of particles migration in laminar as well as turbulent flow. Results and analysis of the velocity profile and particle behavior will be presented and discussed in the following chapters.

Chapter 3. Flow Geometry - Mesh Configuration

In this chapter, the simulation systems adapted in this work is presented, the geometry of the computational domain, mesh configuration, materials that have been employed in the simulation are described.

3.1. Geometry of Computational Domain

To make this work more realistic, a pipe flow, which is one of the most common configurations in industry, with 2 cm in diameter and 80 cm in length (shows in Figure 1) is considered. Pipe flow has already been well studied and people have developed analytical solutions for laminar pipe flow, as well as power-law correlation for fully developed turbulent pipe flow. It's important to note that large eddy simulation (LES) is only valid in three dimensions (3D) and two dimensional (2D) axisymmetry geometries. Hence, by employing a 2D axisymmetry modeling, LES modeling in the future can be employed.

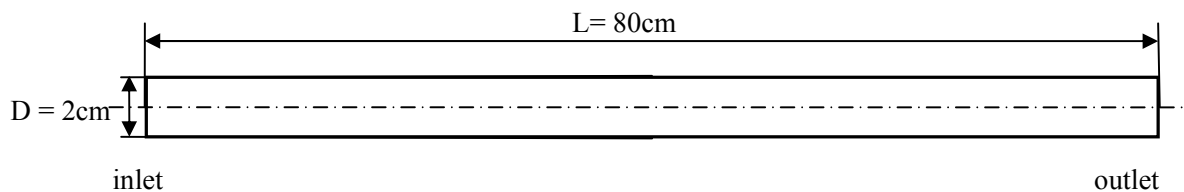


Figure 1. Geometry of Computational Cell

3.2. Mesh Configuration

One of the main purposes of doing this simulation is trying to capture and understand the near wall behavior of nanoparticles, the velocity component perpendicular to the pipe surface, and drag coefficient at the vicinity of pipe wall, therefore a better resolution or a relatively fine mesh in the near wall area or in the boundary layer is needed. However, a low computational effort required that the mesh should not be too fine. As a compromise, a non-uniform quadratic mesh, as illustrated in Figure 2., Is used.

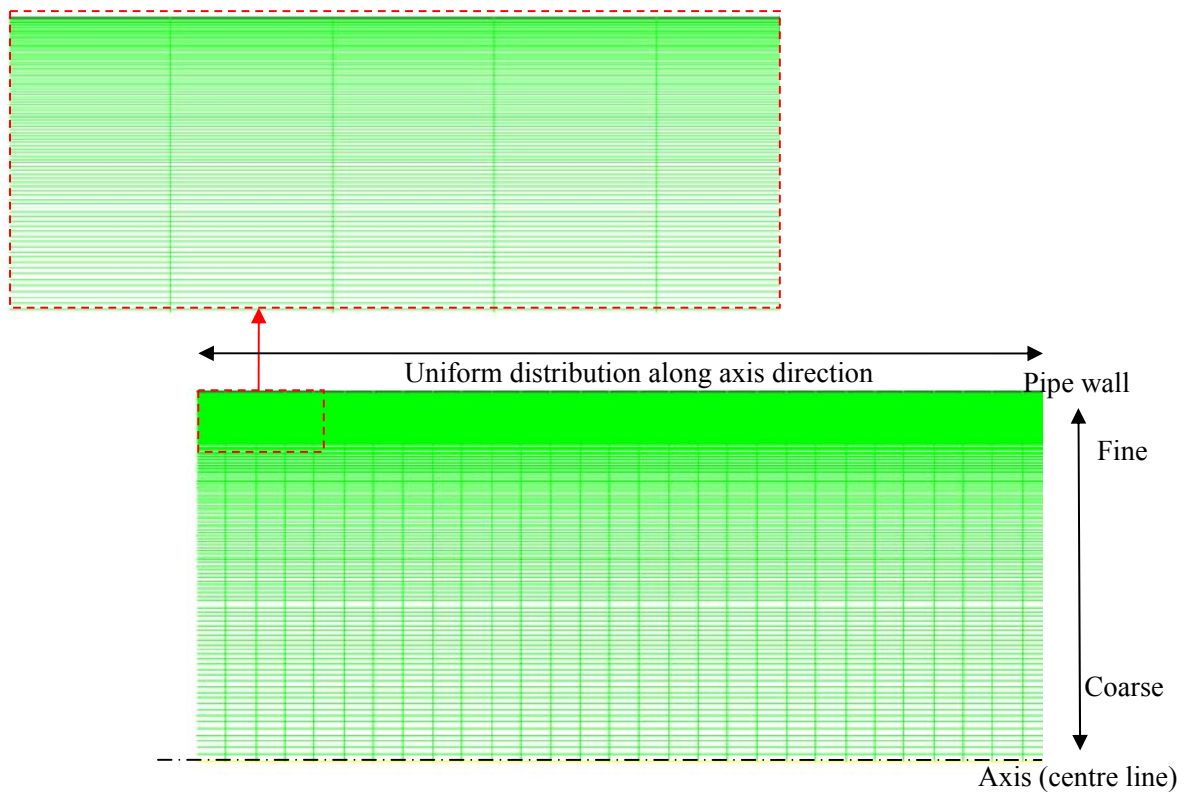


Figure 2. Part of the Mesh of Computational Cell. The mesh in the bottom is part of the pipe mesh, wall and axis are labeled in the figure; the one above is a drawing of partial enlargement of the region encompassed by the red box in the lower image.

In Figure 2, the lower edge corresponds to the axis and the upper edge corresponds to the pipe wall. From the figure, one can observe that there is a very fine mesh at the near wall region and a relatively coarse mesh in the area near the centre line. In Figure 2, there are two images: the mesh in the bottom is part of the pipe mesh, wall and axis are labeled in the figure; the other one is a drawing of partial enlargement of the region encompassed by the dashed box in the lower image. This magnified image is used to give a visual idea of the non-uniform mesh. The two-way arrow on the right side of the mesh is indicating that the mesh becomes finer near the wall, but gradually become coarser when moving toward the centre line.

Another reason for using fewer elements along the axis is that changes of flow properties along the axis is expected to be more gradual, so it's not necessary to employ a fine mesh or non-uniform mesh along the axis direction. Instead, much coarser, uniform mesh is employed along the axis direction.

As it is mentioned above, by employing the idea of axisymmetrical modeling, the computational cell can be simplified to a rectangle with height of 1 cm and length of 80 cm. 1,000 uniform divisions in the axis direction and 200 non-uniform divisions in the radius direction are made. Hence, in total, there are 200,000 elements and 201,201 nodes. The maximum aspect ratio of the elements is around 170 and the maximum cell squish is 0 which means all the elements are rectangle. Other mesh information is summarized in Table 1. The smallest elements, with height of 4.7 μm and length of 800 μm are locate adjacent to the pipe wall, whereas the largest elements with height of 200 μm and length of 800 μm are connected with the centre line.

| Direction | Number of Divisions | Uniform or Non-uniform | Smallest Scale | Largest Scale |
|------------|---------------------|------------------------|---------------------|-------------------|
| Radius (r) | 200 | Non-uniform | 4.707 μm | 200 μm |
| Axis (x) | 1000 | Uniform | 800 μm | 800 μm |

Table 1. Mesh Configuration in Radius and Axis Directions

3.3. Spatial Convergence Test

The sensitivity of the mesh was checked using a coarser mesh, which has 81% of the total number of elements in the original mesh. The number of total elements along each direction is modified to 90% of the original number, which correlates in the radius direction to 180 divisions (compare with 200 for original), and in axis direction to 900 divisions (compare with 1000 for original).

Realizable k - ϵ simulation is applied to a one-phase flow by keeping the same boundary conditions with the same convergence criteria, and the results are shown as below:

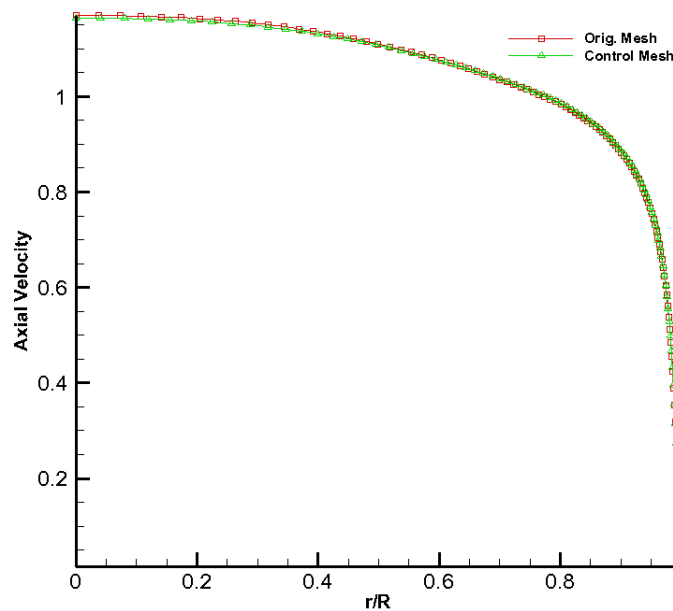


Figure 3. Mesh Sensitivity Check: Comparison of Outlet Axis Velocity

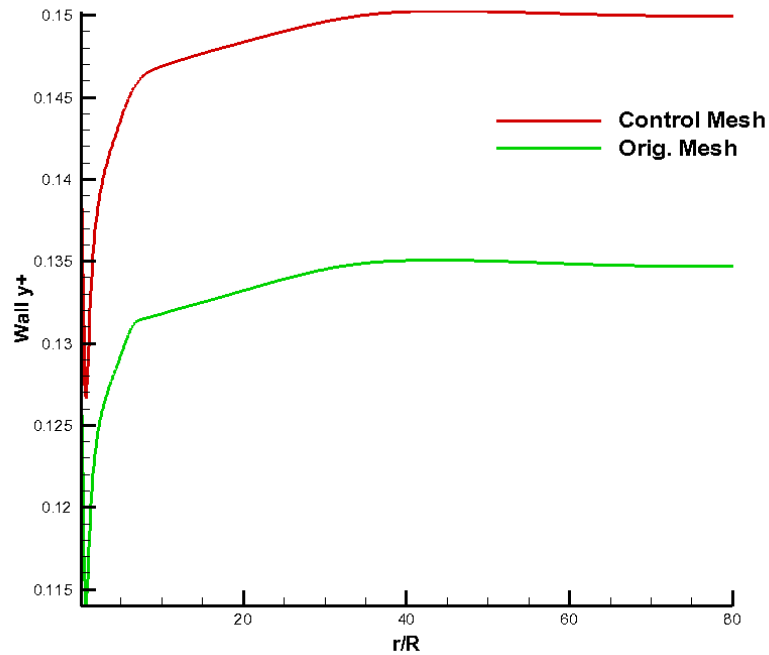


Figure 4. Mesh Sensitivity Check: Comparison of Outlet Axis Velocity

Figure 3 and Figure 4 are showing the mesh sensitivity of our results. Figure 3 is the comparison of the velocity profile at flow outlet ($x=0.8\text{m}$), it shows the velocity profiles of two meshes are overlapping, so the mesh size that adapted here is fine enough. Figure 4 is showing the smallest y^+ , when using a coarse mesh, the y^+ increased from 0.133 to 0.147. This is because the first cell adjacent to the wall is larger.

3.4. Base fluid, Nanoparticles and Pipe

In this present section the properties of the base fluid, nanoparticles and the pipe used in these simulations are discussed. The base fluid used in the serial of simulations is water, and its properties are listed in Table 2. The nanoparticles used in the simulation are spherical carbon particles with diameter of 500 nm, and its properties are listed in Table 3. The pipe is made of aluminum, and its properties are listed in Table 4.

| Base Fluid | Density (kg/m ³) | Viscosity (kg/(m·s)) | Specific Heat (J/(kg·K)) | Thermal Conductivity (W/m·K) |
|------------|---------------------------------|-------------------------|-----------------------------|---------------------------------|
| Water | 998.2 | 0.001003 | 4182 | 0.6 |

Table 2. Properties of Water

| Nanoparticle | Density (kg/m ³) | Diameter (nm) | Thermal Conductivity (W/m·K) |
|--------------|---------------------------------|---------------|---------------------------------|
| Carbon | 2000 | 500 | 0.33 |

Table 3. Property of Nanoparticles (Carbon)

| Pipe Well Material | Density (kg/m ³) | Specific Heat (J/(kg·K)) | Thermal Conductivity (W/m·K) |
|-----------------------|---------------------------------|-----------------------------|---------------------------------|
| Aluminum | 2719 | 871 | 202.4 |

Table 4. Property of Pipe Wall

Chapter 4. Modeling and Results of Laminar Flow

4.1. Laminar Flow(Single Phase)

Fully developed laminar flow, occurs when away from inlets and exits of the pipe where fluid flows in parallel layers, with no disruption between the layers.¹⁶ The velocity for fully developed laminar flow in a pipe can be obtained by solving the Navier-Stokes equations analytically, and the velocity u can be expressed as a function of the radius and the pressure gradient as shown in Eqn. 3, or in terms of the centerline (maximum) velocity U shown in Eqn. 4 in a dimensionless form

$$u = \frac{r^2 - R^2}{4\mu} \left(\frac{\partial p}{\partial x} \right) \quad (3)$$

$$\frac{u}{U} = 1 - \left(\frac{r}{R} \right)^2 \quad (4)$$

Where R is the radius of inner wall, μ is the dynamic viscosity of the fluid.

In 2D axisymmetric geometries, the axial and radial momentum conservation equations are given by:

$$\begin{aligned} \frac{\partial}{\partial t}(\rho v_x) + \frac{1}{r} \frac{\partial}{\partial x}(r \rho v_x v_x) + \frac{1}{r} \frac{\partial}{\partial r}(r \rho v_r v_x) \\ = -\frac{\partial p}{\partial x} + \frac{1}{r} \frac{\partial}{\partial x} \left[r \mu \left(2 \frac{\partial v_x}{\partial x} - \frac{2}{3} (\nabla \cdot \vec{v}) \right) \right] + \frac{1}{r} \frac{\partial}{\partial r} \left[r \mu \left(\frac{\partial v_x}{\partial r} + \frac{\partial v_r}{\partial x} \right) \right] + F_x \end{aligned} \quad (5)$$

$$\begin{aligned} \frac{\partial}{\partial t}(\rho v_r) + \frac{1}{r} \frac{\partial}{\partial r}(r \rho v_r v_r) + \frac{1}{r} \frac{\partial}{\partial x}(r \rho v_r v_x) \\ = -\frac{\partial p}{\partial r} + \frac{1}{r} \frac{\partial}{\partial r} \left[r \mu \left(2 \frac{\partial v_r}{\partial r} - \frac{2}{3} (\nabla \cdot \vec{v}) \right) \right] \\ + \frac{1}{r} \frac{\partial}{\partial x} \left[r \mu \left(\frac{\partial v_x}{\partial r} + \frac{\partial v_r}{\partial x} \right) \right] - 2\mu \frac{v_r}{r^2} + \frac{2}{3} \frac{(\nabla \cdot \vec{v}) \mu}{r} + \rho \frac{v_\theta^2}{r} + F_r \end{aligned} \quad (6)$$

Where

$$(\nabla \cdot \vec{v}) = \frac{\partial v_x}{\partial x} + \frac{\partial v_r}{\partial r} + \frac{v_r}{r} \text{ and } v_\theta \text{ is the swirl velocity which is 0 in our work.}$$

To test the simulation result, a pressure driven flow simulation is conducted by using the mesh described in the previous chapter. The static driven pressure is 13.67 Pascal and the outlet pressure is 0 Pascals. Finite volume method is applied, and the solution is solved by steady-state pressure based solver under SIMPLE-Consistent algorithm described in reference 18.

In the pressure based solver, the continuity (Eqn. 7) and momentum equations (Eqn. 8) in integral form are listed below:

$$\oint \rho \vec{v} \cdot d\vec{A} = 0 \quad (7)$$

$$\oint \rho \vec{v} \vec{v} \cdot d\vec{A} = -\oint \rho I \cdot d\vec{A} + \oint \bar{\tau} I \cdot d\vec{A} + \int_V \vec{F} \cdot dV \quad (8)$$

Where

I is the identity matrix, $\bar{\tau}$ is the stress tensor, and \vec{F} is the force vector.

The momentum equations are discretized as below:

$$a_p u_i = \sum_{nr} a_{nr} u_{inr} + \sum p_f A \cdot \hat{i} + S \quad (9)$$

Where the subscript nr stands for neighboring cells, u_i is one of the velocity components (u_x, u_y, u_z), a_p is the linear coefficient for u_i , a_{nr} is coefficient for the neighboring cells, p_f is the pressure at the surface between the two adjacent cells. This value of p_f can be

obtained by a second-order upwinding interpolating procedure described below in Eqn. 10:

$$p_f = p + \nabla p \cdot \vec{r} \quad (10)$$

Then the continuity equation is integrated over a control volume and yield the discrete equation as shown in Eqn.11.

$$\sum_f^N \rho \vec{v}_n A_f = 0 \quad (11)$$

Where N is the total face number, ρ is the density of the material and \vec{v}_n is the velocity components, hence $\rho \vec{v}_n$ is the mass flux through the face.

Then the face values of velocity \vec{v}_n are related to the values of velocity at the centers of the small volumes. However, in order to avoid “checkerboarding” described by Rhie and Chow¹⁷, a momentum-weighted averaging is adapted, and the coefficient a_p is used as a weighting factor. After this, the face flux $\rho \vec{v}_n$ can be expressed as Eqn.10:

$$\rho \vec{v}_n = \rho_f \frac{a_{p,c_0} v_{n,c_0} + a_{p,c_1} v_{n,c_1}}{a_{p,c_0} + a_{p,c_1}} + d_f \left(\left(p_{c_0} + (\nabla p)_{c_0} \cdot \vec{r}_0 \right) - \left(p_{c_1} + (\nabla p)_{c_1} \cdot \vec{r}_1 \right) \right) \quad (12)$$

The equations are solved by a “segregated algorithm”. In this segregated algorithm, the individual governing equations for the solution variables (in this laminar 2D case the variables are u, v and p) are solved one by one. Each governing equation, while being solved, is “decoupled” from other equations. The segregated algorithm is memory-efficient, since the discretized equations need only be stored in the memory once

at a time. However, the solution convergence is relatively slow, as the equations are solved in a decoupled manner.¹⁸ The 6 steps in each iteration are illustrated below in Figure 5:

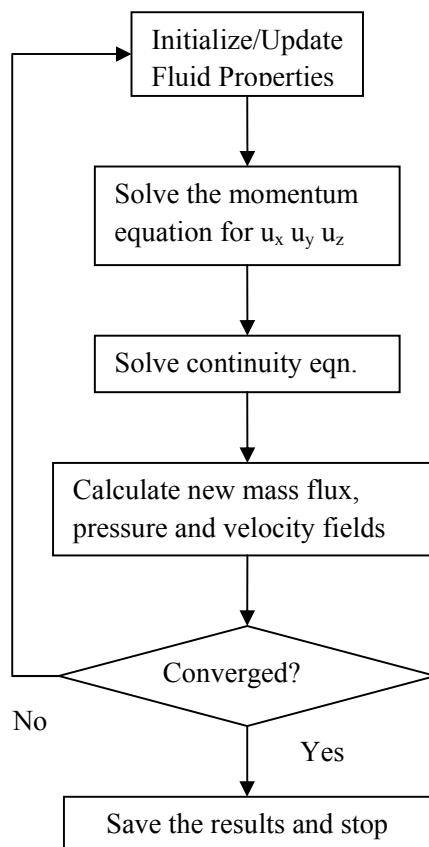


Figure 5. Flow Chart of Pressure-based Algorithm Used in Fluid Solver

The simulation results together with analytical solution are posted in Figure 6. The velocity term u is nondimensionalized by the centre line velocity U computed from the simulation, while the radius is nondimensionalized by the radius of the pipe. From the figure, one can observe a parabolic velocity profile. A comparison of both the simulation

and analytical models shows that these models agree very well with each for single phase flow.

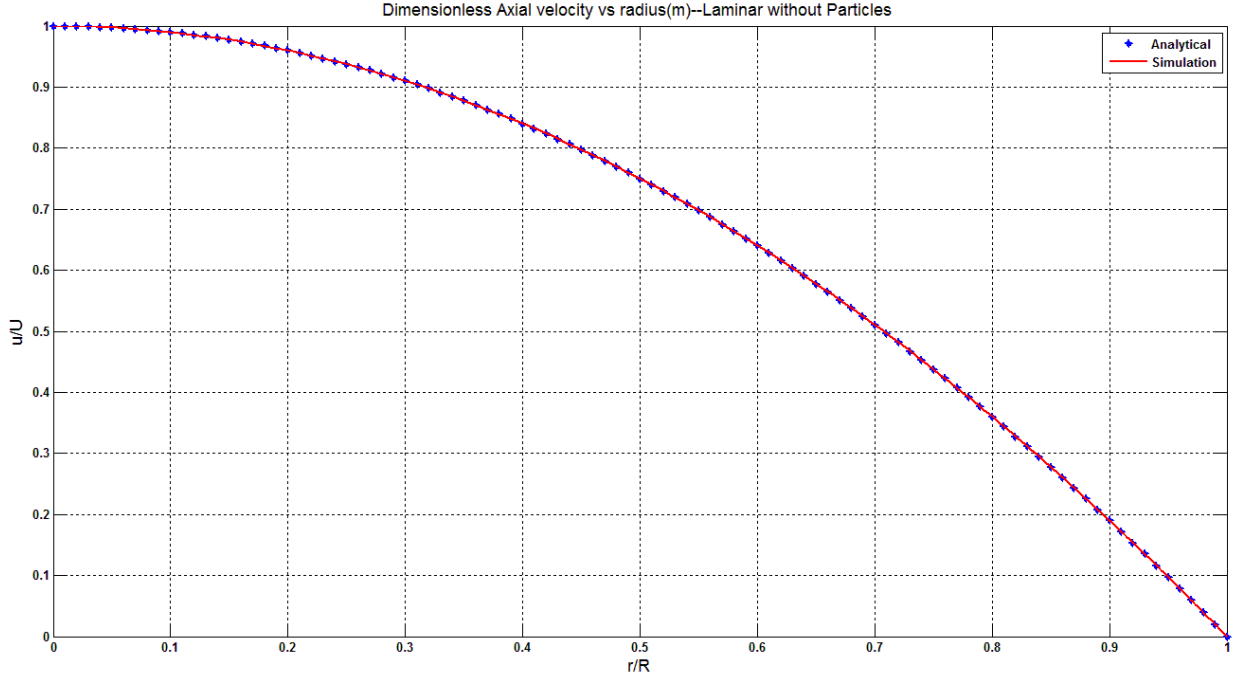


Figure 6. Comparison between Analytical Solution and Simulation Results: Axial Velocity Profile of Fully Developed Laminar Flow (Dimensionless)

The mass flow rate can be computed from the simulation data by using interpolation and numerical integration as described in Eqn.13. Then the Reynolds Number can be computed through applying Eqn.14.

$$\dot{m} = \iint_S \rho v dS \quad (13)$$

$$Re = \frac{\rho \bar{v} D}{\mu} \quad (14)$$

Where \bar{v} is the mean velocity of fluid, D is the diameter of the pipe, S corresponds to the surface of pipe cross section. Following the two equations Eqn. 13 and

Eqn. 14, the mass flow rate is computed as $\dot{m} = 0.008000$, the average velocity $\bar{v} = 0.02551071$ and Reynolds Number $Re_D = 507$ which is lower than the laminar to turbulent transition Reynolds Number where $Re_D = 2,300$ ¹⁹.

4.2. Particle Tracking in Laminar Flow by Eulerian-Lagrangian Method

In this part the particle tracking theory in Eulerian-Lagrangian approach is discussed. Eulerian-Lagrangian approach is where only the main fluid is treated as a continuum, using Eulerian description. The governing equations for the main fluid phase are Navier-Stokes equations, and they are solved by numerical method such as finite difference, finite volume or finite element. However, the dispersed particles are tracked by using the Lagrangian description, and particles can exchange momentum, mass, and energy with the main fluid phase.

4.2.1. Two-way Coupling

The modeling is done under assumptions and configurations listed below:

1). Particle-particle interaction is ignored. In this problem, dilute fluid is considered in modeling, the volume fraction of the dispersed particles is less than 2%, and particles are uniformly injected into the continuum phase (water). Since the volume fraction of the injected particles is relatively low, it's appropriate to ignore the particle-particle interaction.

2). "Two-way coupling" is employed in our modeling. "Coupling" refers to the simultaneous solution of Eulerian and Lagrangian fields. Generally speaking, there are two types of coupling. The first approach, also a simpler approach, is "one-way coupling", in which particles behaviors are calculated based on a fixed continuous phase flow field. In this approach, the flow field is solved to a well converged solution, then the particles

are added and the trajectories and other properties of those particles are calculated. Hence, the addition of particles will not impact the solution of fluid field. The other approach is “Two-way coupling”, where the continuum phase can affect the behavior of discrete phase (particles), and vice versa. Hence, in this process a proper designed solver will calculate the continuous and discrete phase equations in an alternate manner until a converged coupled solution is achieved.

4.2.2. Equations of Motion for Particles

As it is mentioned earlier, the moving of the discrete phase (particles) is handled in the Lagrangian domain. The trajectories of particles are calculated by an integrating method. The force balance on the discrete phase is integrated, and the force balance should be equal to the particle inertia with forces acting on the particles. Finally, the equation of motion of particles can be written as Equ.15 (take x direction as an example):

$$F_{drag}(u - u_p) + F_x = \frac{du_p}{dt} m_p \quad (15)$$

Here u_p is the velocity of the particle, u is the velocity of fluid, m_p is the mass of particle, F_x is the sum of other forces acted on particle (such as Brownian force and gravity) and $F_{drag}(u - u_p)$ is the drag forces acted on the particle, where,

$$F_{drag} = \frac{Re C_D}{24} \frac{18\mu}{\rho_p d_p^2} m_p \quad (16)$$

Where C_D is the drag coefficient, μ is the molecular viscosity of base fluid, ρ is the density of fluid, ρ_p is the density of particle, d_p is the particle diameter, and Re is the relative Reynolds Number

$$Re = \frac{|u_p - u| \rho d_p}{\mu} \quad (17)$$

4.2.3. Integration of Particle Motion Equation

Eqn.15 can be integrated and an analytical expression of the particle velocity at next step u_p^{n+1} can be found in the form of:

$$u_p^{n+1} = e^{\frac{-\Delta t F_{drag}}{m_p}} \left(u_p^n - u^n \right) - \frac{m_p a_{total}}{F_{drag}} \left(e^{-\Delta t F_{drag}} - 1 \right) + u^n \quad (18)$$

Here, the acceleration term a_{total} is the summation of all other accelerations except that caused by drag.

Remember the velocity of particle is defined as:

$$u_p = \frac{dx}{dt} \quad (19)$$

Eqn. 18 can be integrated again to obtain an analytical solution of the particle location at n+1 time step x_p^{n+1} :

$$x_p^{n+1} = \Delta t \left(u_p^n + \frac{m_p}{F_{drag}} a_{total} \right) + \frac{m_p}{F_{drag}} \left(1 - e^{-\frac{F_{drag} \Delta t}{m_p}} \right) \left(u_p^n - u^n - a_{total} \frac{m_p}{F_{drag}} \right) + x_p^n \quad (20)$$

and in Eqn 20, u_p^n and u^n are the particle velocity and fluid velocity at previous location, respectively.

Despite the analytical approach, the particle velocity and location can also be solved by using numerical discretization schemes such as trapezoidal discretization, Euler implicit discretization, and Runge-Kutta scheme²⁰.

4.2.4. Modeling the Drag Coefficients

The continuum phase can affect the discrete phase behavior through drag. There are two drag laws that may be useful in our simulation, one is spherical drag law and the other is the Stokes-Cunningham Drag Law. In our studies, both of these two laws were studied and the results were compared.

The first one is the spherical drag law suggested by Morsi and Alexander²¹ in 1972. They studied the drag of particles in several different models, and finally derived an empirical expression of the drag coefficient for smooth spherical particles in fluid described with different Reynolds Number from 0.1 to 50,000. In their studies, they used particles with diameter from 10 to 100 μm , and studied particles' response to one-dimensional flow, collision with a cylinder, and collision with a lifting airfoil. They claimed that the drag coefficients calculated from their equations are within 1-2% of experimental results. Their drag-Reynolds-Number relationship for spherical particles is shown in Eqn.19:

$$C_D = k_1 + \frac{k_2}{\text{Re}} + \frac{k_3}{\text{Re}^2} \quad (21)$$

Where Re is the Reynolds Number of the fluid, k_1 , k_2 and k_3 are three empirical constants that may vary with Re. The values of these constants are listed below in Table 5:

| Range of Reynolds Number Re | Expression of Drag Coefficient C _D |
|-----------------------------|---|
| Re < 0.1 | 24/Re |
| 0.1 < Re < 1.0 | 22.73/Re + 0.0903/Re ² + 3.69 |
| 1.0 < Re < 10.0 | 29.1667/Re - 3.8889/Re ² + 1.222 |
| 10.0 < Re < 100.0 | 46.5/Re - 116.67/Re ² + 0.6167 |
| 100.0 < Re < 1000.0 | 98.33/Re - 2778/Re ² + 0.3644 |
| 1000.0 < Re < 5000.0 | 148.62/Re - 4.75 × 10 ⁴ /Re ² + 0.357 |
| 5000.0 < Re < 10000.0 | -490.546/Re + 57.87 × 10 ⁴ /Re ² + 0.46 |
| 10000.0 < Re < 50000.0 | -1662.5/Re + 5.4167 × 10 ⁶ /Re ² + 0.5191 |

Table 5. Drag-Reynolds-Number Relationship

The second drag law that may be valid is the Stokes-Cunningham Drag Law suggested by Ounis et al²² in 1991. They studied drag of particles with diameter from 0.01 to 0.1 μm, and showed that the Brownian effects play a significant role in the diffusion of submicrometer particles at distances less than 2 wall units from the solid surface.

Their expression for the drag acting on an individual particle is:

$$F_D = \frac{18\mu}{d_p^2 \rho_p C_c} \quad (22)$$

Where F_D is the drag per unit particle mass and C_c is Cunningham correction to Stokes' drag law which can be obtain from Eqn.23:

$$C_c = 1 + \frac{2\lambda}{d_p} \left(1.257 + 0.4e^{-\frac{1.1d_p}{2\lambda}} \right) \quad (23)$$

In Eqn.23, λ is molecular mean free path, which means the mean travel distance per collision, and can be calculated from Serway's²³ approach:

$$\lambda = \frac{\bar{v}t}{\pi d_p^2 \bar{v} t n_v} = \frac{1}{\pi d_p^2 n_v} \quad (24)$$

Where n_v is the number of molecules per unit volume, \bar{v} is the average velocity of the travelling molecule.

4.2.5. Momentum and Mass Exchanges

In the two way coupling approach, the configuration of the discrete phase can affect the continuum phase by exchanging momentum and mass with the continuum.

The momentum exchange should be calculated and passed to the momentum equation of the continuum as an additional momentum source term. The momentum source term generated by the discrete particles can be written as Eqn. 25:

$$Mum_p = \sum \left(\frac{18\mu C_{drag} Re}{24d_p^2 \rho_p} (u_p - u) + F_{other} \right) \dot{m}_p \Delta t \quad (25)$$

Where Re is the relative Reynolds number, F_{other} stands for additional force, such as gravitational force and Brownian force. Finally, this momentum source term will appear in the momentum equations of fluid and affect the solution of momentum equations for the continuum.

Despite the momentum exchange, the discrete phase can affect the continuum by passing additional mass exchange term to the momentum equations, and this term can be evaluated through Eqn. 26.

$$M = \frac{\Delta m_p}{m_{p,0}} \dot{m}_{p,0} \quad (26)$$

This mass exchange term will be passed to the continuous equation of continuum as a mass source term, so it will finally affect the continuity solution of the fluid.

4.2.6. Brownian Motion

Brownian motion is a random motion of sub-micrometer particles inside a fluid, and it is caused by the geometrically unequal hit of the small fluid molecules on the particle surface. Usually, the Brownian motion is regarded as discovered by the botanist Robert Brown in 1827.

One computational scheme used to include Brownian motion into simulation was developed by Li A and Ahmadi G²⁴ in 1993. In their work, the components of the Brownian force are modeled as a Gaussian white noise random process and the Brownian force is modeled as Eqn.27:

$$F_{Br} = m_p G_i \sqrt{\frac{\pi S_0}{\Delta t}} \quad (27)$$

where m_p is the mass of the particle, G_i is unit variance zero mean Gaussian random numbers obtained from a pair of random numbers N_1 and N_2 from the range $[0, 1]$ and Δt is the time step used in the simulation. S_0 is given by Eqn.28:

$$S_0 = \frac{216\nu k_B T}{\pi \rho d_p^5 \left(\frac{\rho_p}{\rho}\right)^2 C_C} \quad (28)$$

Where T is the absolute temperature of the fluid, ν is the kinematic viscosity of fluid, and k_B is the Boltzmann constant which is 1.38×10^{-23} J/K, other terms like C_C and ρ are still as the same meaning as is defined in previous chapters.

4.2.7. Simulation Configurations

Two simulations were done with nano-particles injected at 1% mass flow rate (0.4% volume fraction) of the fluid with both Brownian force included and excluded. After that, particles with injection of 2.0 % mass flow rate (1% volume fraction) of water are studied without Brownian force. The boundary conditions for the continuum are:

1. Inlet: Plug flow with velocity of 0.0255 m/s parallel to axis, which means the mass flow rate of water (density is 988kg/m^3) is 0.008 kg/s, and the correspond Reynolds number is 507.
2. Outlet: Relative pressure equal to 0 Pascal;
3. Wall: Stationary wall without slip;
4. Axis: Axisymmetry;

Boundary conditions for the dispersed particles are:

1. Inlet: 100 uniformly distributed particle injections with total
2. Outlet: Relative pressure equal to 0 Pascal;
3. Wall: Stationary wall, particles hit the wall will reflect;
4. Axis: Axisymmetry;

In the simulation, the solver completes 150 flow iterations per discrete phase iteration. Regarding the integration time step of the moving particles, 0.005 sec is used. Hence, in the total domain, the particle motion equations are evaluated no less than 1600 times, and this makes sure the velocity of those particles are updated when they traveled about one cell distance.

4.2.8. Results and Discussion for Laminar Eulerian-Lagrangian Approach

The axial velocity profile of fluid at various locations (cross sections, $x = 0.0$ m, $x = 0.2$ m, $x = 0.4$ m, $x = 0.6$ m and $x = 0.8$ m) are shown in Figure 7. In that figure, it can be observed that the changing of the flow velocity profiles. Plug flow is present at $x=0$ m, while parabolic profiles show up at the outlet $x=0.8$ m. Velocity terms are non-dimensionalized by the center line velocity at the pipe outlet where $x=0.8$ m, and the radius are non-dimensionalized by the radius of the pipe which is 0.01m.

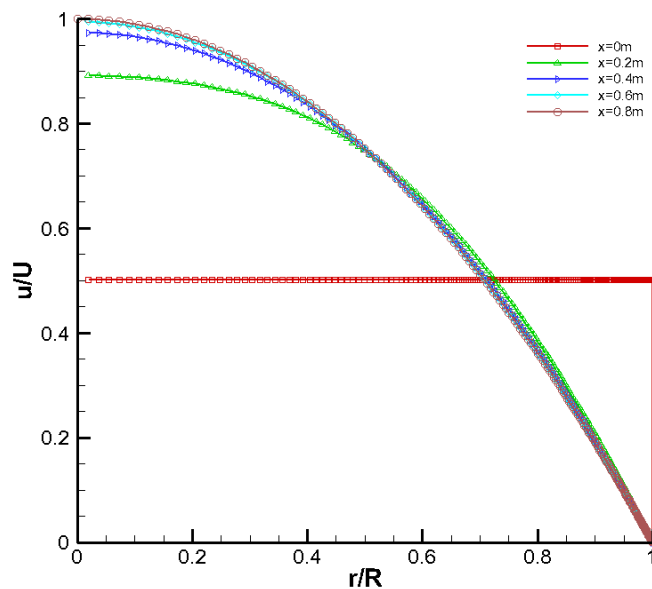


Figure 7. Dimensionless Velocity Profile of Fluid at Different Cross-sections ($x=0.0$ m, $x=0.2$ m, $x=0.4$ m, $x=0.6$ m and $x=0.8$ m) in Laminar Pipe Flow with Particles Injection of 1% volume fraction, exclude Brownian Force.

Velocity profiles at different cross sections of both cases (fluid only and flow with particles injections) are compared in Figure 8. At the pipe inlet, the velocity profiles for both cases are exactly the same. At downstream locations ($x=0.4$ m and 0.8 m) the center part velocity for pure fluid is greater than that of flow with particle injections, but in the near wall region the velocity of flow with particles is larger than that of flow without particles.

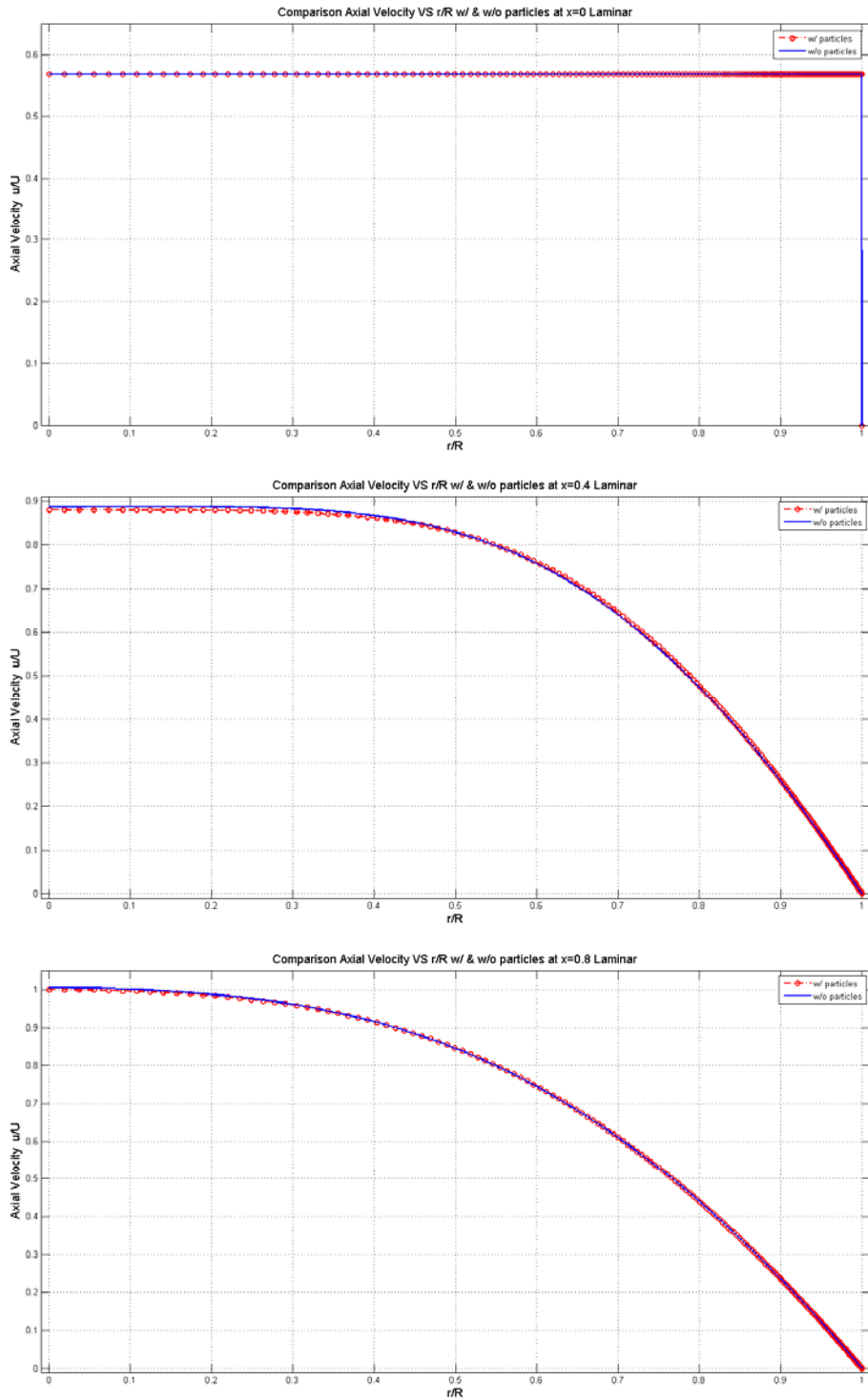


Figure 8. Comparison of Velocity Profiles for Both Cases (with and without Particles Injections) at Different Cross-sections ($x=0.0\text{m}$, $x=0.4\text{m}$ & $x=0.8\text{m}$), Laminar Flow without Brownian Force

To better present the intersection of the two lines of each cases, the intersection points are enlarged and showed in Figure 7.

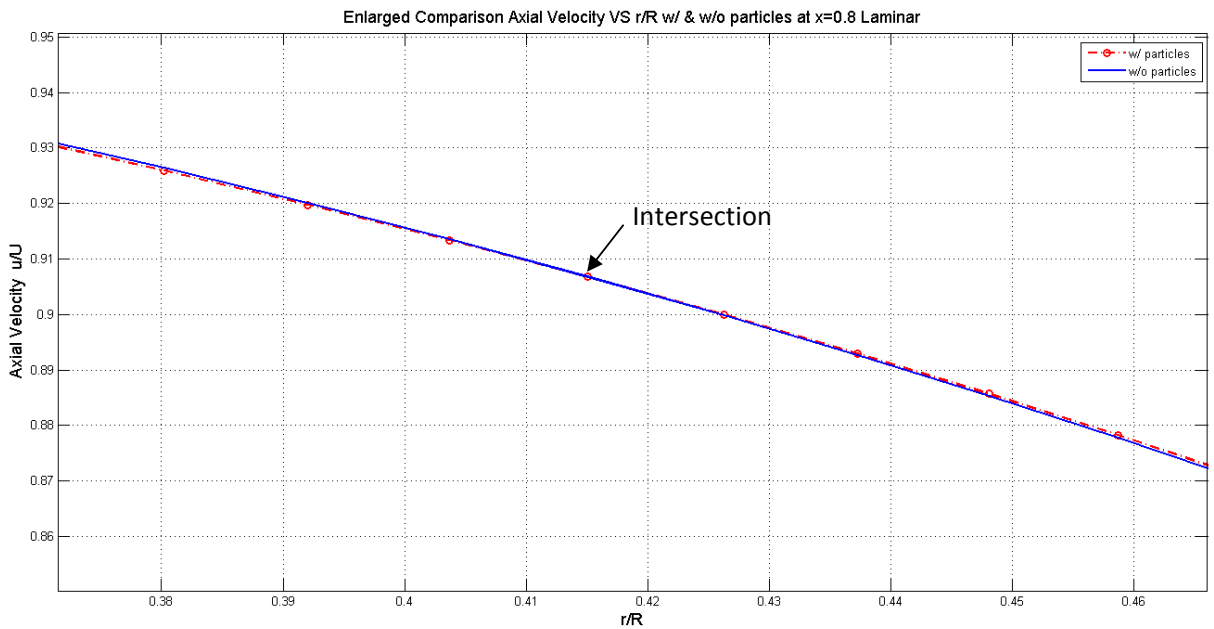
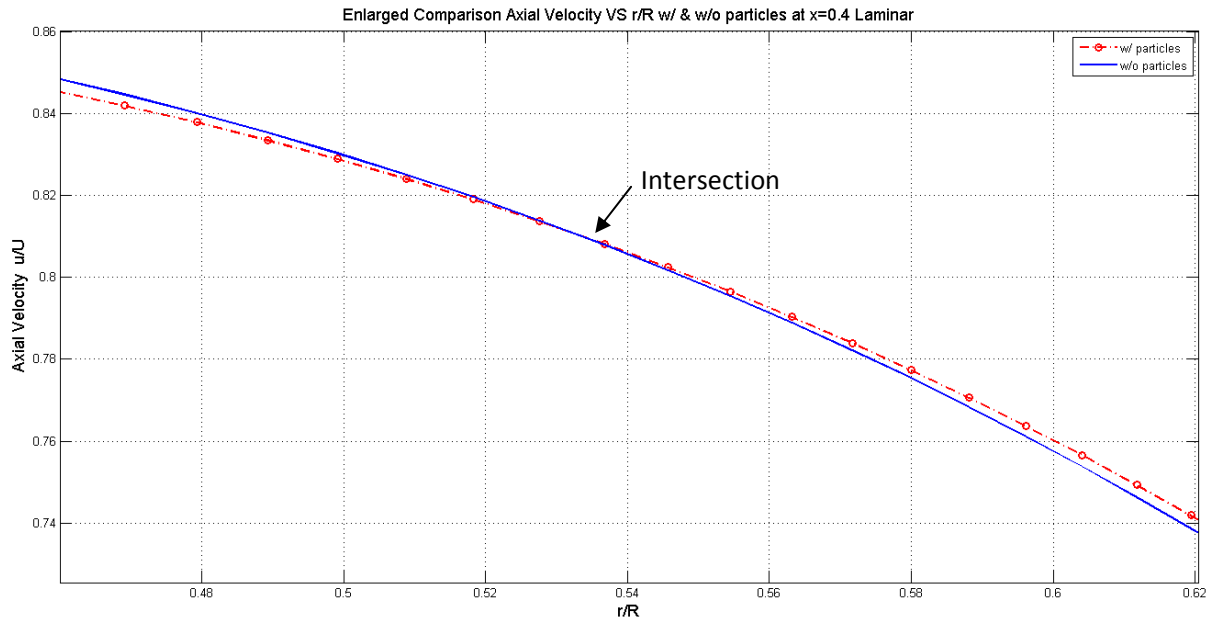


Figure 9. Enlarged Figure, Showing the Intersection of the Velocity Profiles of Flow with and without Particle Injections at $x=0.4m$ and $x=0.8m$

One possible reason may be the presence of more particles in the center region, hence occupying certain volume, interacting with fluid, and slowing down the speed of fluid in this region.

As aforementioned, Ding and Wen, 2004¹⁴, claimed that “particle concentration in the wall region can be much lower than that in the central core region.” Beside their work, Lam et al.²⁵ studied micron-sized particles migration in concentrated suspensions, they found that particle concentration was the lowest at the wall, rapidly increased to the maximum at $r/R \sim 0.8 - 0.9$, but decreased slightly towards the pipe centre. Their usage of concentrated suspensions of particles of several microns accounts for differing results in comparison to ours. In their study, the decrease of concentration near the center may due to the shear-thinning effect.

Although, partially similar results were obtained as both groups: in the near wall region the concentration is lower than that in the center region. Despite the similarities, there are some differences between our results and other groups'. In our results, the concentration of particles in the near wall region ($r/R > 0.9$) is greater than the concentration of particles in the region between the wall and center ($0.15 < r/R < 0.9$). This may be the results of the missing Brownian force. In Ding and Wen¹⁴ model they included Brownian force which may have very important effect in the near wall boundary layer region, and the claimed that Brownian motion has an effect of redistribution of particles between higher concentration regions to lower concentration regions. Hence, if Brownian force was added to the laminar models, it may help with distributing the particles in the near wall region to the region a little far from the wall. Another reason should be numerical error at those two cells.

25 particle trajectories at different locations are presented in

Figure 10 below. The trajectories are colored by particles velocities, where red stands for the highest velocity, and blue is associated with the slowest velocity.

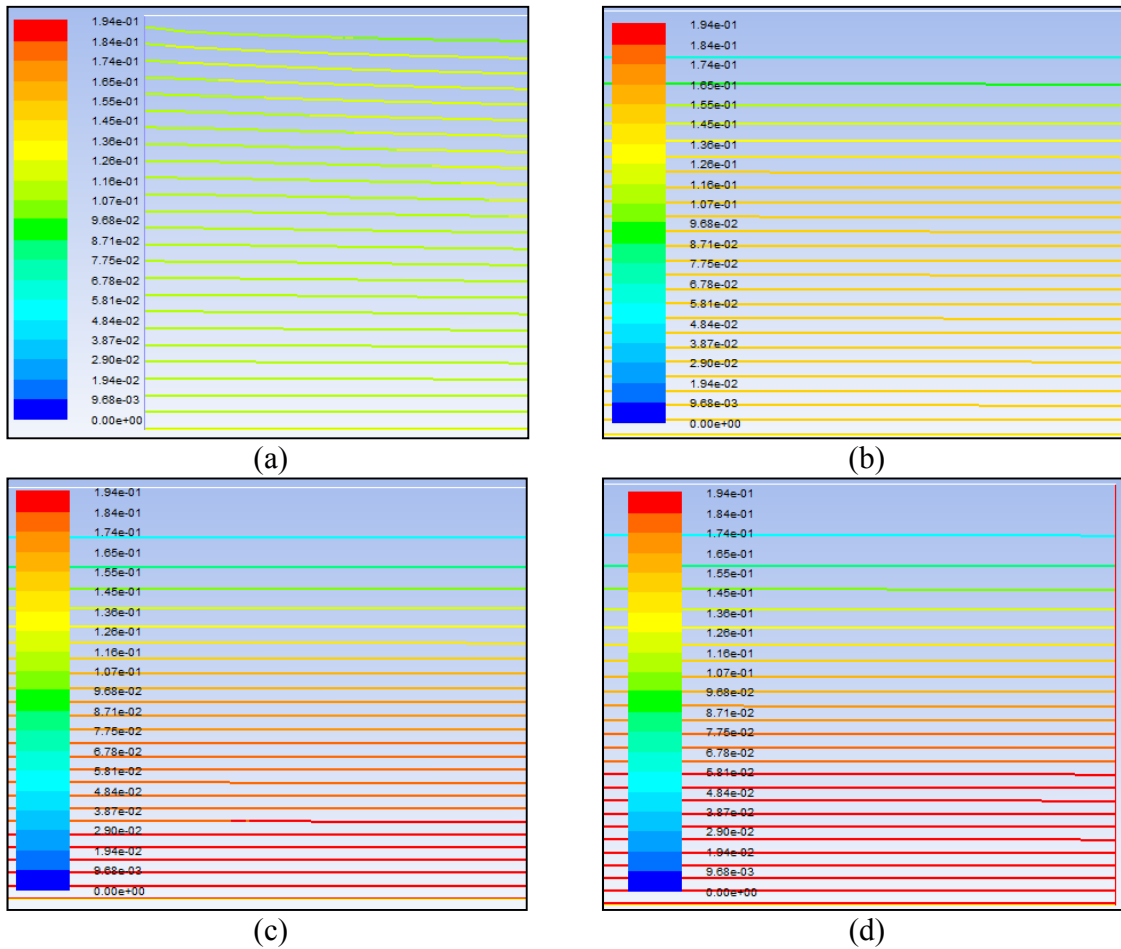


Figure 10. Trajectories are colored by velocity magnitude. a) Particles are uniformly released from the pipe inlet, where $x=0m$; b) Trajectories of 25 particles at downstream where x is around 0.2m; c) Trajectories of 25 particles at downstream where x is around 0.6m; d) Trajectories of 25 particles at the pipe out let, where $x=0.8m$

These figures are showing that at the beginning 25 particles are uniformly injected at the pipe inlet, but as they are going downstream, the particles begin to slightly moving toward the center line (lower surface of the pipe). Compare the first figure a) with the last

figure (d), it can be found that the tracked particles are shifting toward the center line.

This can also be verified by the histogram of particle locations showing below:

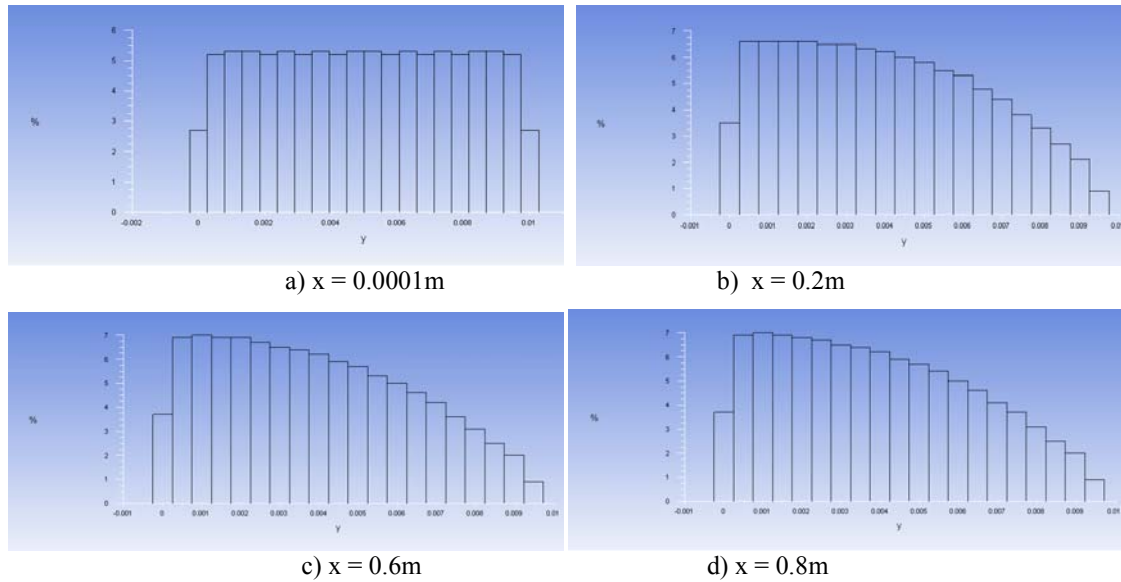


Figure 11. Histogram of Particle Locations Histogram of Particle Locations at Varies Cross sections for Laminar Flow with Plug Flow Inlet

The simulation for fully developed laminar pipe flow is also conducted. The flow profile at the pipe inlet has a parabolic velocity profile with center line velocity equals 0.15 m/s, and the velocity profile can be expressed as below:

$$u(r) = \left(1 - \frac{r^2}{R^2}\right) \cdot U_{center} \quad (29)$$

Where R is the radius of the pipe which is 0.01m, and U_{center} is the center line velocity 0.15 m/s.

In these models Saffman's Lift Force²⁶ is included. Saffman's Lift Force is a force or lift caused by shear. This idea of this lift force is proposed by Saffman in 1965, after that Li and Ahmadi²⁷ in proposed the expression for this force in 1992. In the particles balance equations Eqn.13, the Saffman's Lift Force term described in Eqn.25 is given by:

$$\vec{F} = \frac{2(\vec{v} - \vec{v}_p) \rho K \sigma_{ij} \sqrt{v}}{\rho_p d_p (\sigma_{lk} \sigma_{kl})^{\frac{1}{4}}} \quad (30)$$

Where σ_{ij} is the deformation tensor, K is a constant K=2.594, and Re is the relative Reynolds number, which is defined as Eqn.17. The particle trajectories are presented in Figure.12:

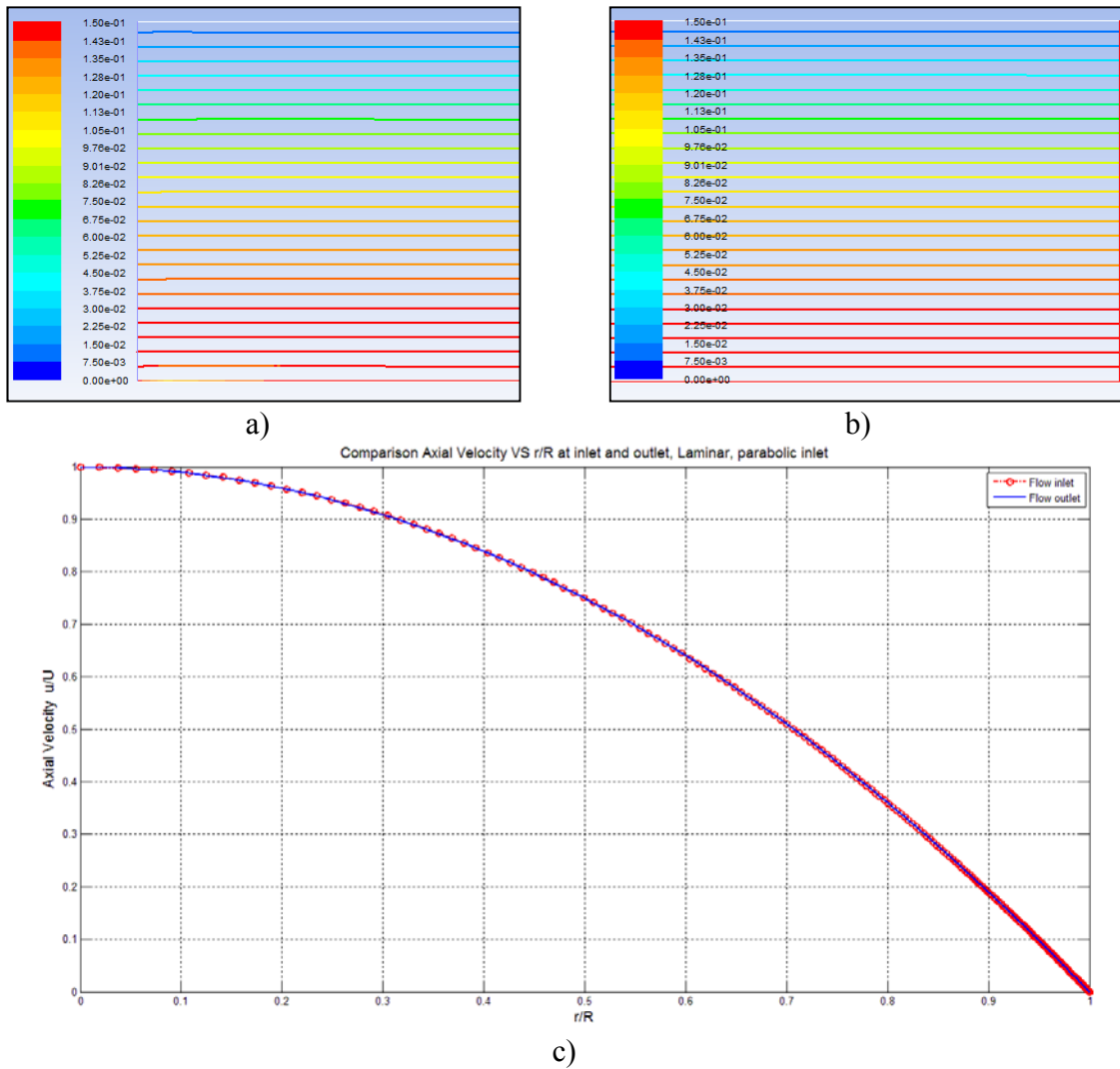


Figure 12. Particle trajectories for fully developed laminar flow: a) pipe inlet, x=0m; b) pipe outlet, x=0.8m; c) Comparison of Axial Velocity at Inlet and Outlet

To better illustrate the result, four histograms showing the particle percentage at varies cross sections are shown below:

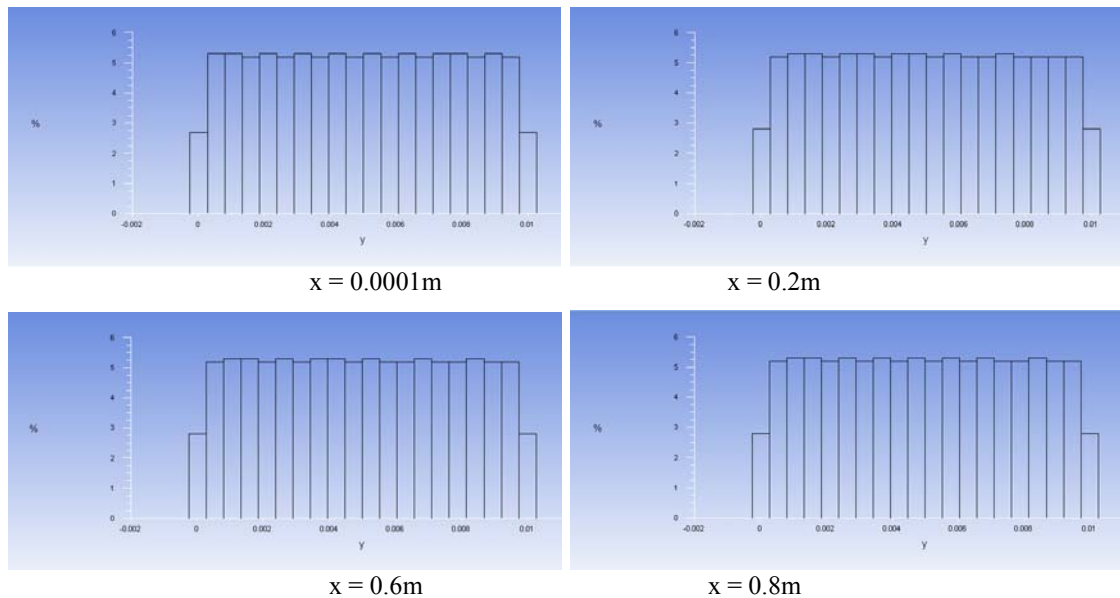


Figure 13. Histogram of Particle Locations at Varies Cross Sections for Laminar Pipe Flow with Fully Developed Parabolic Inlet

From Figure 12 and Figure 13 it is found that the particles are going along a straight line and parallel to the pipe wall. The velocity of the particles is similar to that of a vicinal fluid. This result is different from that of Ding and Wen¹⁴. The possible reason is that, the dispersed particles in their model are treated as continuous phase and they included Brownian motion in their model. By treating the particle as a continuous phase, it's clear that they are using the Eulerian-Eulerian description which may result in a different solution. The other possibility is the Brownian force may help with distribute the particles at the near wall region. However, comparing the time scale of Brownian motion and fluid time scale, it can be concluded that Brownian effects are not realizable

in these flows. Because the Brownian motion often has a time scale as low as 10^{-2} seconds, but fluid time scale in our case is about 30 seconds.

Chapter 5. Modeling and Results of Turbulent Pipe Flow

In this chapter the theory of turbulent flow and governing equations used in turbulent pipe flow are presented. Afterward, particle tracking scheme will be provided, and finally simulation results of particles migration in turbulent pipe flow will be presented and discussed.

5.1. Turbulent Flow(Single Phase)

Turbulent flow is one in which the fluid particles rapidly mix as they move along due to random three dimensional velocity fluctuations. Due to turbulence's random, three dimensional, chaotic and stochastic nature, analytical solution for turbulent flow are not available. Hence, in the turbulent regime semi-empirical theories are used to model the flow.

In pipe flow, typical transition Reynolds Number of flow from laminar flow to turbulence is 2,300.¹⁹ The velocity profile for fully developed turbulent pipe flow through a smooth pipe is shown in Figure 14 . Another famous and widely used description of turbulent velocity profile for pipe is the “power-law”, the expression are presented in Eqn.31 below.

$$\frac{\bar{u}}{U} = \left(1 - \frac{r}{R}\right)^{\frac{1}{n}} \quad (31)$$

Where U is the center line velocity of the pipe flow, R is the radius of the pipe and n is a component that can vary with different Reynolds Number, its expression is:

$$n = -1.7 + 1.8 \log \text{Re}_U \quad (32)$$

The expression of Reynolds number for pipe flow is:

$$\text{Re}_{D_h} = \frac{\rho V D}{\mu} = \frac{V L}{\nu} \quad (33)$$

Regarding the usage of the power, in practice, $n=7$ is frequently applied. The velocity profile expression for $n=7$ is called “one-seventh power law”, and it’s frequently used to represent the velocity profile of fully developed turbulent pipe flow.

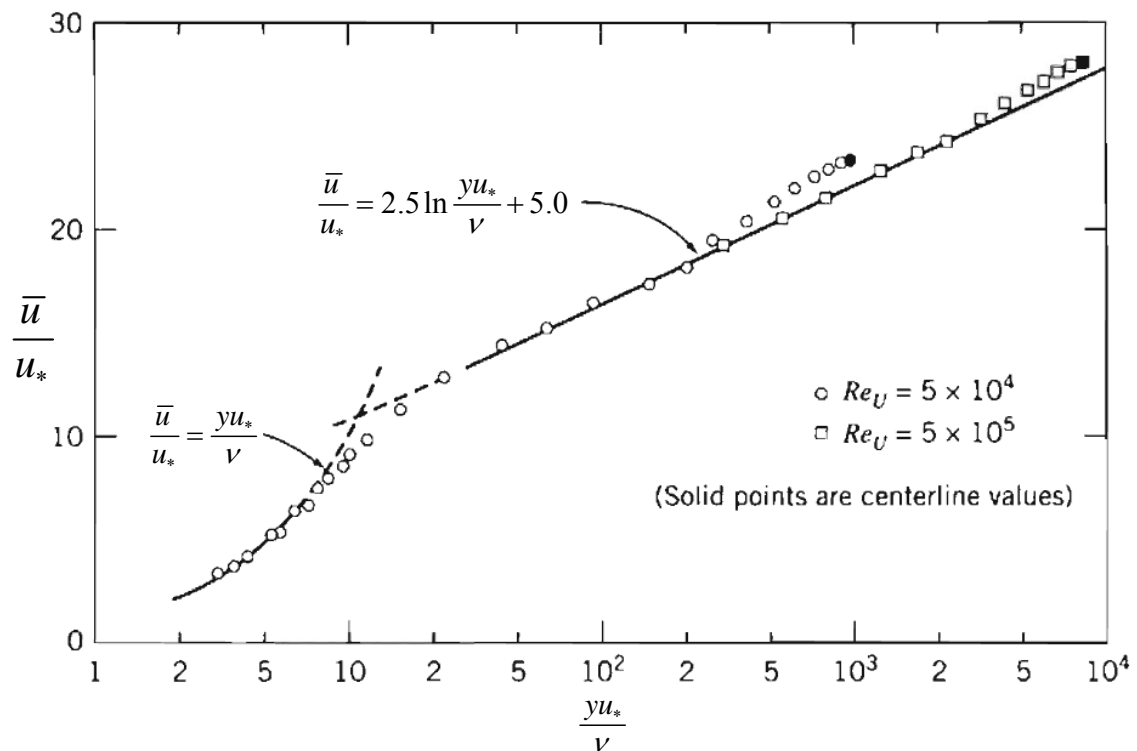


Figure 14. Turbulent Velocity Profile for Fully Developed Flow in a Smooth Pipe. (Adapted from reference [19])

5.2. Reynolds-averaged Navier-Stokes (RANS) Equations and k-ε Model

Solutions of the Navier-Stokes (N-S) equations for high Reynolds-number turbulent flows in complex geometries require to resolve from the largest eddies all the way down to the smallest scales of the motion (Kolmogorov's scale). In some cases, especially in complex geometry, it's unlikely to achieve a solution in a certain time. In order to overcome this problem, some alternative methods were introduced by researchers, such as Reynolds-averaged Navier-Stokes. In this thesis, the k-ε model, a branch RANS method, is applied.

RANS are time-averaged equations of motion for fluid flow. It's generated by using Reynolds decomposition. In this model, all instantaneous quantities are divided into two parts: time-averaged and fluctuating quantities. Which means the instantaneous quantities ϕ should be divided as $\phi = \bar{\phi} + \phi'$, where $\bar{\phi}$ is the time-averaged part and ϕ' is the fluctuating part. Applying such decomposition to all the quantities, substituting them into the instantaneous continuity and momentum equations and taking ensemble average yields:

$$\frac{\partial \rho}{\partial t} + \frac{\partial}{\partial t}(\rho u_i) = 0 \quad (34)$$

$$\frac{\partial}{\partial x_j}(\rho u_i u_j) + \frac{\partial}{\partial t}(\rho u_i) = -\frac{\partial p}{\partial x_i} + \frac{\partial}{\partial x_j} \left[\mu \left(\frac{\partial u_i}{\partial x_j} + \frac{\partial u_j}{\partial x_i} - \frac{2}{3} \delta_{ij} \frac{\partial u_l}{\partial x_l} \right) \right] + \frac{\partial}{\partial x_j} \left(-\overline{\rho u_i' u_j'} \right) \quad (35)$$

These two equations above are so called RANS equations. In equation (35), the term $\left(-\overline{\rho u'_i u'_j}\right)$ is so called Reynolds stresses, and usually it is related to the mean velocity gradients through the use of Boussinesq assumptions²⁸:

$$\left(-\overline{\rho u'_i u'_j}\right) = \mu_t \left(\frac{\partial u_i}{\partial u_j} + \frac{\partial u_j}{\partial u_i}\right) - \frac{2}{3} \delta_{ij} \left(\rho k + \mu_t \frac{\partial u_k}{\partial u_k}\right) \quad (36)$$

Where μ_t is the turbulent eddy viscosity, k is the turbulence kinetic energy.

There are several models developed by using RANS, some widely used are k- ϵ , k- ω , Reynolds stress model (RSM) and v^2 -f models. Detailed description of k- ϵ model is presented in next section.

5.3. k-ε Model

k-ε model is proposed by Launder and Spalding in 1972²⁹. In the k-ε model, besides the typical momentum and continuity equations, there are two additional equations used to describe turbulence properties. The two equations are transport equations for turbulent kinetic energy - k, and turbulent dissipation rate - ε. In our simulation the Realizable k-ε model proposed by T.-H. Shih, et al³⁰ is used. Equations for k and ε are shown below:

$$\frac{\partial}{\partial x_j}(\rho k u_j) + \frac{\partial}{\partial t}(\rho k) = G_k + G_b - \rho \varepsilon - Y_M + S_k + \frac{\partial}{\partial x_j} \left[\left(\mu + \frac{\mu_t}{\sigma_k} \right) \frac{\partial k}{\partial x_j} \right] \quad (37)$$

$$\frac{\partial}{\partial x_j}(\rho \varepsilon u_j) + \frac{\partial}{\partial t}(\rho \varepsilon) = \rho C_1 S \varepsilon - \rho C_2 \frac{\varepsilon^2}{k + \sqrt{\nu \varepsilon}} + C_{1\varepsilon} C_{3\varepsilon} G_b \frac{\varepsilon}{k} + S_\varepsilon \quad (38)$$

Where $C_1 = \max \left[0.43, \frac{\mu}{\mu + 5} \right]$, $\mu = S \frac{k}{\varepsilon}$, $S = \sqrt{2 S_{ij} S_{ij}}$

In the above equations,

(1) $\mu_t = \rho C_\mu \frac{k^2}{\varepsilon}$ is the eddy viscosity and $C_\mu = \frac{1}{A_0 + A_s \frac{k U_*}{\varepsilon}}$

here $U_* = \sqrt{S_{ij} S_{ij} + \tilde{\Omega}_{ij} \tilde{\Omega}_{ij}}$

and $\tilde{\Omega}_{ij} = \Omega_{ij} - 2 \varepsilon_{ijk} \omega_k$

$$\Omega_{ij} = \bar{\Omega}_{ij} - \varepsilon_{ijk} \omega_k$$

Here A_0 and A_s are constants, $A_0=4.04$ and $A_s = \sqrt{6} \cos \phi$, $\bar{\Omega}_{ij}$ is the mean rate-of-rotation tensor viewed in a rotating reference frame with angular velocity ω_k . Other values mentioned are:

$$C_{1\varepsilon} = 1.44, \quad C_2 = 1.9, \quad \sigma_k = 1.0, \quad \sigma_\varepsilon = 1.2$$

Among the above constants, σ_k and σ_ε are the turbulent Prandtl numbers for k and ε , respectively, $C_{1\varepsilon}$ and C_2 are model constants. The rest of the quantities are given below:

$$\phi = \frac{\cos^{-1}(W\sqrt{6})}{3}, \quad W = \frac{S_{ij}S_{jk}S_{ki}}{\tilde{S}^3}, \quad \tilde{S} = \sqrt{S_{ij}S_{ij}}, \quad S_{ij} = \frac{1}{2} \left(\frac{\partial u_j}{\partial x_i} + \frac{\partial u_i}{\partial x_j} \right)$$

(2) G_k is the generation of turbulence kinetic energy due to the mean velocity gradients:

$$G_k = -\overline{\rho u'_i u'_j} \frac{\partial u_j}{\partial x_i} \xrightarrow{\text{apply Boussinesq hypothesis}} G_k = \mu_t S^2$$

Where S is the modulus of the mean rate-of-strain tensor and $S = \sqrt{2S_{ij}S_{ij}}$

(3) G_b is the generation of turbulence kinetic energy due to buoyancy, and Y_M represents the contribution of the fluctuating dilatation in compressible turbulence to the overall dissipation rate, S_k and S_ε are additional source terms for k and ε , respectively, all these terms (G_b , Y_M , S_k and S_ε) are null for our case.

Finally, by using k - ε model, the two equations for turbulent kinetic energy - k , and turbulent dissipation rate - ε , will be solved together with the continuity equation and two momentum equations described in section 4.1..

5.4. Stochastic Tracking of Particles - Random Walk Model

Unlike tracking particles in laminar flow model, tracking particles in turbulent model requires consideration of turbulent dispersion of particles. With Reynolds decomposition of flow quantities such as $u = \bar{u} + u'$, particles can be tracked only based on the mean flow velocity \bar{u} . However, to better represent the chaotic and stochastic nature of turbulence, the effect of instantaneous turbulent velocity fluctuations u' on particles trajectories should be included. One wide used model is the Random Walk Model. This model was first introduced by Karl Pearson³¹, who established the discipline of mathematical statistics, in 1905 and it is widely used in many fields now.

5.4.1. Integration Time

In order to predict the turbulent dispersion of particles, the trajectory equations for individual particles will be integrated, using the instantaneous fluid velocity, $\bar{u} + u'$, along the particle path. The integration time is defined as the time spent in turbulent motion along a small particle path ds , and given as Eqn.39 below:

$$T = \int_0^{\infty} \frac{u_p'(t)u_p'(t+s)}{u_p'^2} ds \quad (39)$$

For small “tracer” particles (marker) that move with the fluid (no drift velocity), the integral time becomes the fluid Lagrangian integral time, T_L . For k-ε model, T_L can be obtained by matching the diffusivity of tracer particles, $\overline{u_i' u_j'} T_L$, to the scalar diffusion

rate predicted by the turbulence model $\frac{V_t}{\sigma}$. The resultant expression for T_L is given by

$T_L \approx 0.15 \frac{k}{\varepsilon}$. This is only valid for k- ε model.

5.4.2. Discrete Random Walk Model

In the random walk model, particles will interact with a succession of discrete stylized eddies, and those eddies are characterized by their own time scale, τ_e , and three velocity fluctuation terms u' , v' and w' .

Firstly, in order to give a more realistic description of the correlation function, the characteristic eddy life time, τ_e , is defined as $\tau_e = -T_L \ln(\xi)$ instead of using constants as $2T_L$. ξ is a random number that is uniformly distributed between 0 and 1. The particle will interact with an eddy until the eddy dies out or the particle traveled out of the eddy. With the eddy life time τ_e is already known, the “eddy escaping time” is required to be determined for a particle escape from a eddy. It can be defined as:

$$\tau_{\text{escape}} = -\tau \ln \left[1 - \left(\frac{L_e}{\tau |u - u_p|} \right) \right] \quad (40)$$

Where τ is the particle relaxation time and L_e is the eddy's length scale.

Secondly, the chaotic turbulent fluctuation terms should be modeled. One way to generate the random fluctuation terms u' , v' and w' , is through assuming the fluctuation terms obey the Gaussian probability distribution given by Eqn.44 below:

$$f(x) = \frac{1}{\sqrt{2\pi\sigma^2}} e^{-\frac{(x-\mu)^2}{2\sigma^2}} \quad (41)$$

In the simulation, it's assumed that the fluctuation terms are randomly distributed, and can be represented as below:

$$u' = \zeta \sqrt{u'^2}, \quad v' = \zeta \sqrt{v'^2}, \quad w' = \zeta \sqrt{w'^2} \quad (42)$$

Where ζ is a normally distributed number; and the left root mean square terms are associated with the kinetic energy at each local point. By assuming an isotropic turbulent flow, one can define:

$$\sqrt{u'^2} = \sqrt{v'^2} = \sqrt{w'^2} = \sqrt{\frac{2k}{3}} \quad (43)$$

5.5. Simulation Configurations

Our work is concentrated on studying the particle migrations in turbulent flow, more simulations were done in the part. Simulations were done for suspensions with different concentrations. All simulations for steady state k-ε turbulent models are discussed and summarized in Table 6 and below:

| Case No. | Laminar Or Turbulent | Particle Size | Volume Fraction % | Reynolds Number Re | Mass flux \dot{m} (kg/s) | Mean Velocity U (m/s) | Inlet Boundary Cotions | Outlet Boundary Conditions |
|----------|----------------------|---------------|-------------------|--------------------|----------------------------|-----------------------|------------------------|----------------------------|
| 1 | Turbulent | 0 nm | 0% | 19560 | 0.3081683 | 0.98269909 | Fully Developed* | Pressure is 0 |
| 2 | Turbulent | 100 nm | 1% | 19560 | 0.3081683 | 0.98269909 | Fully Developed | Pressure is 0 |
| 3 | Turbulent | 200 nm | 1% | 19560 | 0.3081683 | 0.98269909 | Fully Developed | Pressure is 0 |
| 4 | Turbulent | 500 nm | 1% | 19560 | 0.3081683 | 0.98269909 | Fully Developed | Pressure is 0 |
| 5 | Turbulent | 500 nm | 2% | 19560 | 0.3081683 | 0.98269909 | Fully Developed | Pressure is 0 |
| 6 | Turbulent | 500 nm | 5% | 19560 | 0.3081683 | 0.98269909 | Fully Developed | Pressure is 0 |
| 7 | Turbulent | 500 nm | 10% | 19560 | 0.3081683 | 0.98269909 | Fully Developed | Pressure is 0 |
| 8 | Turbulent | 1 μm | 1% | 19560 | 0.3081683 | 0.98269909 | Fully Developed | Pressure is 0 |
| 9 | Turbulent | 2 μm | 1% | 19560 | 0.3081683 | 0.98269909 | Fully Developed | Pressure is 0 |
| 10 | Turbulent | 5 μm | 1% | 19560 | 0.3081683 | 0.98269909 | Fully Developed | Pressure is 0 |
| 11 | Turbulent | 5 μm | 5% | 19560 | 0.3081683 | 0.98269909 | Fully Developed | Pressure is 0 |

Note*: The Fully developed flow boundary conditions are obtained through the process described in section 5.5

Table 6. Boundary Conditions for Turbulence Cases of Varies Particles Concentrations

The boundary conditions for the continuum (water) are:

1. Inlet: To obtain the fully developed velocity, k and ε profile, the boundary condition described below is applied as the inlet boundary condition and these profiles are used as a initial gauss for the flow field:

- a) The axis velocity component, u, is assumed to obey the 1/7th power law:

$$u = u_{free} \left(1 - \frac{r}{R} \right)^{\frac{1}{7}} \quad (44)$$

Where u_{free} is taken as 1.19 m/s.

- b) The turbulent kinetic energy is assumed to be constant in the free stream, but vary linearly from a near-wall value to the free stream

$$\begin{cases} k_{nw} = \frac{(u_\tau)^2}{\sqrt{C_\mu}} & \text{for where } 0 < r < \delta \\ k_{free} = \frac{(u_{free})^2}{500} & \text{for where } \delta \leq r \end{cases} \quad (45)$$

Where the friction velocity and wall shear take the forms:

$$u_\tau = \sqrt{\frac{\tau_w}{\rho}} \quad \text{and} \quad \tau_w = \frac{f \rho u_{free}^2}{2} \quad (46)$$

Where f is the Moody factor that estimated from the Blasius equation:

$$f = 0.045 \cdot \left(\frac{\delta u_{free}}{\nu} \right)^{-\frac{1}{4}} \quad (47)$$

- c) The dissipation rate is given by the equation below:

$$\varepsilon = \frac{C_\mu^{\frac{3}{4}} \cdot k^{\frac{2}{3}}}{\ell} \quad (48)$$

Where the mixing length ℓ is the minimum of κr and 0.085δ . (κ is the von Karman constant = 0.41.)

2. Outlet: Relative pressure equal to 0 Pascal, back flow turbulent kinetic energy and turbulent kinetic energy dissipation rate is the same as defined at the pipe inlet.
3. Wall: Stationary wall without slip;
4. Axis: Axisymmetry;

Boundary conditions for the dispersed particles are:

1. Inlet: In all these cases, there are 200 particle injections located at $x=0$, one injection point at each cell. The mass flow rate are scaled by the surface area.

2. Outlet: Relative pressure equal to 0 Pascal;
3. Wall: Stationary wall, particles hit the wall will reflect;
4. Axis: Axisymmetry;

The solver completes 200 flow iterations per discrete phase iteration. Regarding the integration time step of the moving particles, a time step around 0.00016 sec is used.

The fully developed velocity, k and ϵ profiles are shown in the figure below:

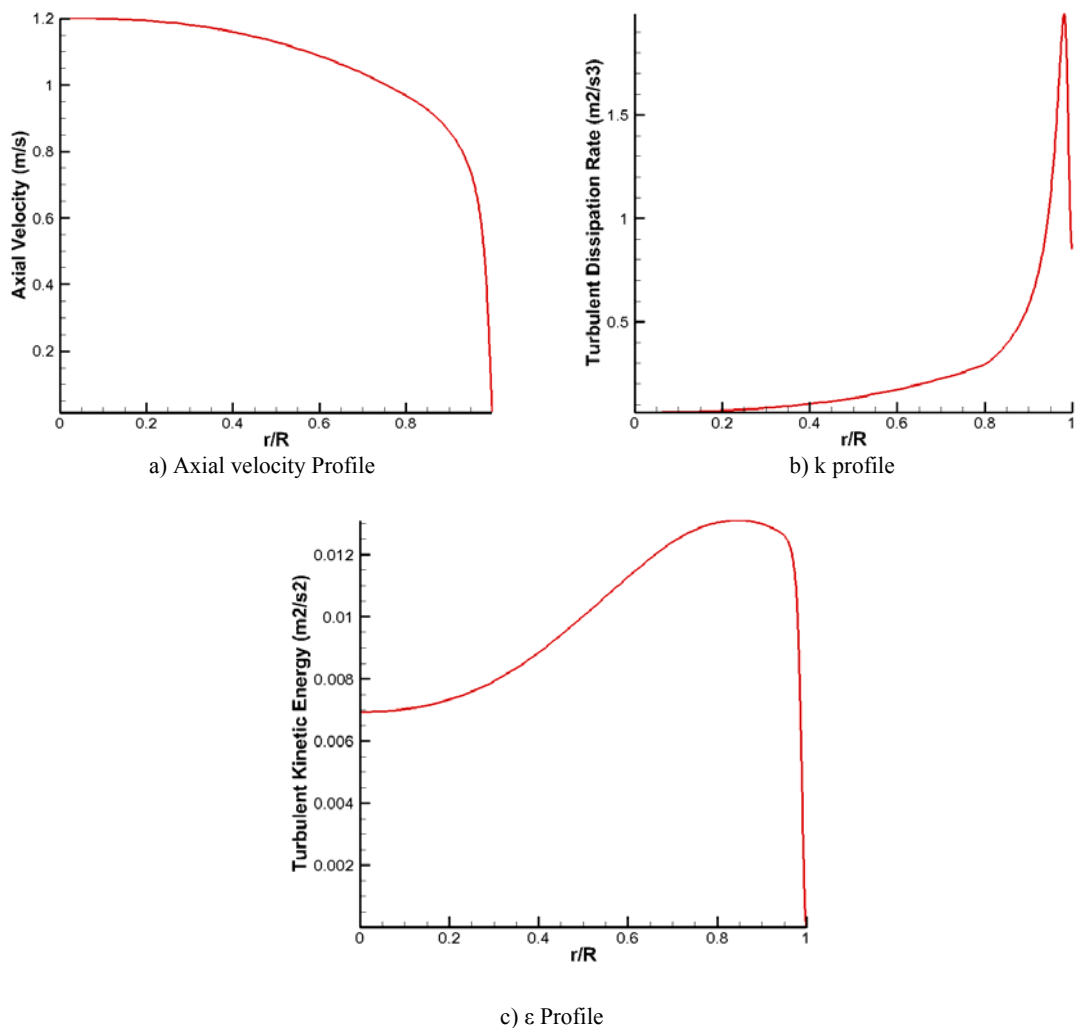


Figure 15. Boundary Conditions of Axial Velocity u , k and ϵ at Pipe Inlet

5.6. Results and Discussion of Particle Migration in Turbulent Flow under k-ε model

Suspensions of particles with different concentrations (1%, 2%, 5% and 10%) were modeled under the realizable k-ε model. Particles used in these simulations are spherical particles with diameter of 500 nm, 200 nm and 100 nm, respectively. All of those particles are released with zero velocity from 200 uniformly distributed injection points which are located at the pipe inlet (x=0.0 m). The release flow rate is proportional to the surface area. In the following paragraph the simulation results will be discussed.

5.6.1. Effect on Friction

The presence of nanoparticles has some effect on the friction factor. The results are showed in Table 7:

| Case No. | Laminar Or Turbulent | Particle Size | Volume Fraction % | Injection Type | Reynolds Number Re | Mass flux \dot{m} (kg/s) | Mean Velocity U (m/s) | Skin Friction Coefficient C_f | Moody Friction Factor f |
|----------|----------------------|---------------|-------------------|----------------|--------------------|----------------------------|-----------------------|---------------------------------|-------------------------|
| 1 | Turbulent | 0 nm | 0% | - | 19560 | 0.3081683 | 0.98269909 | 0.00573824 | 0.02295297 |
| 2 | Turbulent | 100 nm | 1% | Uniform | 19560 | 0.3081683 | 0.98269909 | 0.00583355 | 0.02333419 |
| 3 | Turbulent | 200 nm | 1% | Uniform | 19560 | 0.3081683 | 0.98269909 | 0.00578691 | 0.02314764 |
| 4 | Turbulent | 500 nm | 1% | Uniform | 19560 | 0.3081683 | 0.98269909 | 0.00578081 | 0.02312325 |
| 5 | Turbulent | 500 nm | 2% | Uniform | 19560 | 0.3081683 | 0.98269909 | 0.00579221 | 0.02316884 |
| 6 | Turbulent | 500 nm | 5% | Uniform | 19560 | 0.3081683 | 0.98269909 | 0.00591912 | 0.02367646 |
| 7 | Turbulent | 500 nm | 10% | Uniform | 19560 | 0.3081683 | 0.98269909 | 0.00599977 | 0.02399909 |

Table 7. Nanoparticles Effect on Friction Coefficient and Moody Coefficient Factor

The moody friction factor f for fully developed pipe flow can be estimated by the empirical correlation shown in Eqn.49:

$$f = \frac{0.316}{\text{Re}^{0.25}} \quad (49)$$

Applying the correlation of Eqn.49, it gives a result of Moody coefficient factor equal to 0.0267. When compare with our simulation result which is 0.0229, the error is about 14%.

From the moody friction factors listed in Table 7, the presence of nanoparticles can increase the friction factor. When the concentration is low (1%), the increase is small, but with concentrations as high as 10%, the increase is about 5%. This may be due to the reason that nanofluids have a higher effective viscosity than that of the base fluid. From case 2 to 4, the particle diameter increased, but the skin friction coefficient only changed a little. This means the skin friction is not so sensitive to the particle size.

From case 4 to case 7, the volume fraction of nanoparticles is increased. Compare the friction factor of these 4 cases, a relatively large increase in friction is observed, and the increase of the friction coefficient is proportional to the particle concentrations.

5.6.2. Particles Location

The histograms of particle concentration at different cross sections for several cases are shown below. In the histograms, the y axis is the percentage of particles and the x axis corresponds to the radius r .

a. Histograms for case 1: 100 nm particles, 1% volume fraction:

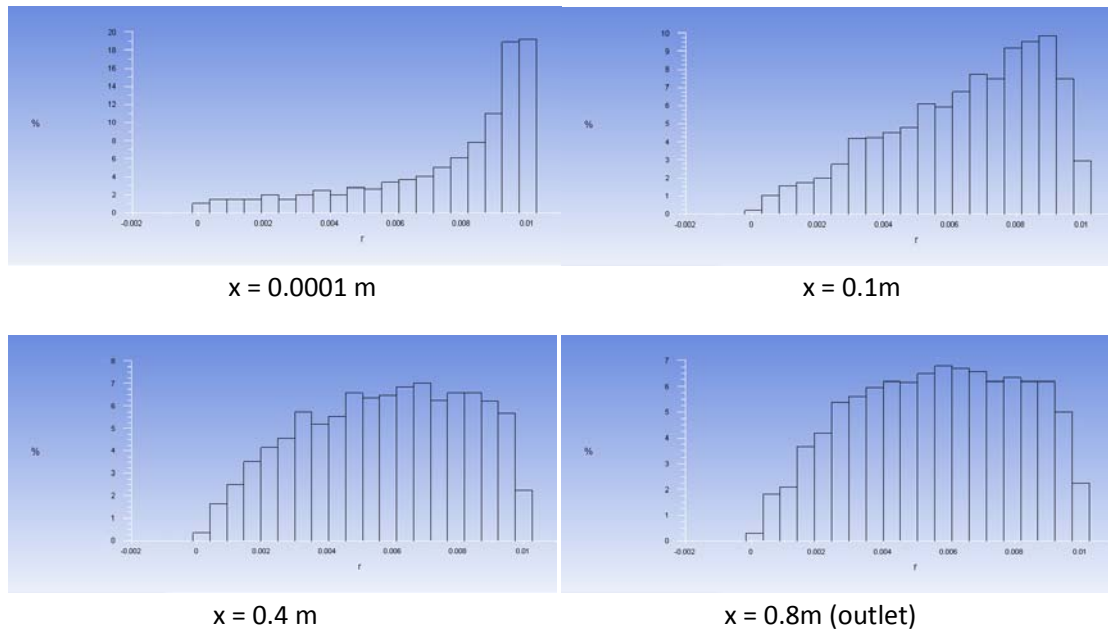
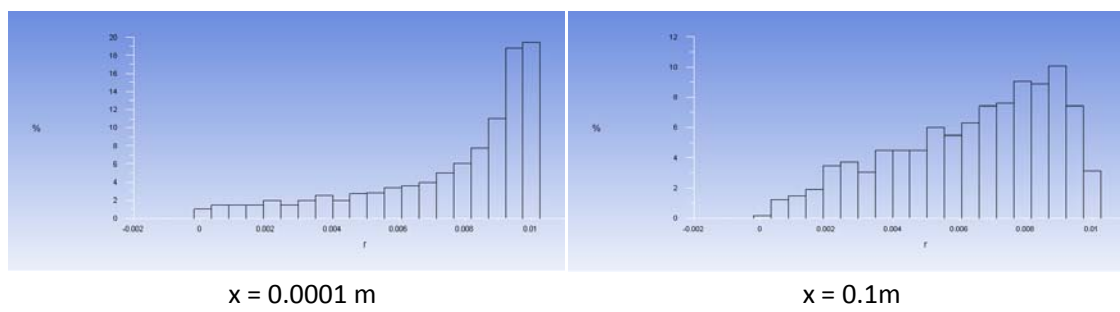


Figure 16. Histograms of Particle Locations at Various Cross Sections for Case 2

b. Histograms for case 4: 500 nm particles, 1% volume fraction:



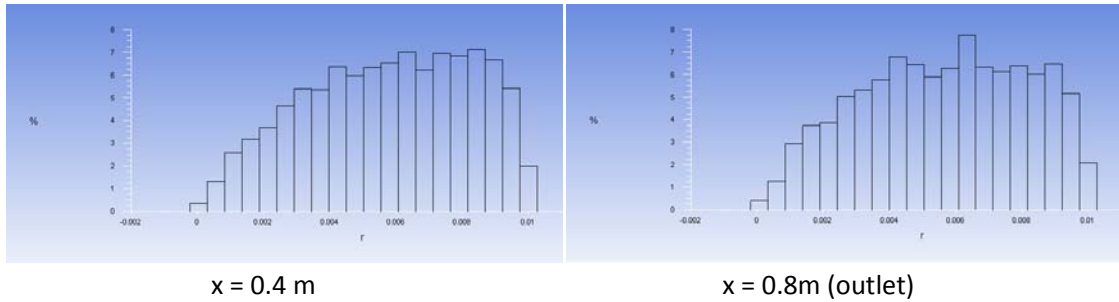


Figure 17. Histograms of Particle Locations at Various Cross Sections for Case 4

c. Histograms for case 7: 500 nm particles, 5% volume fraction:

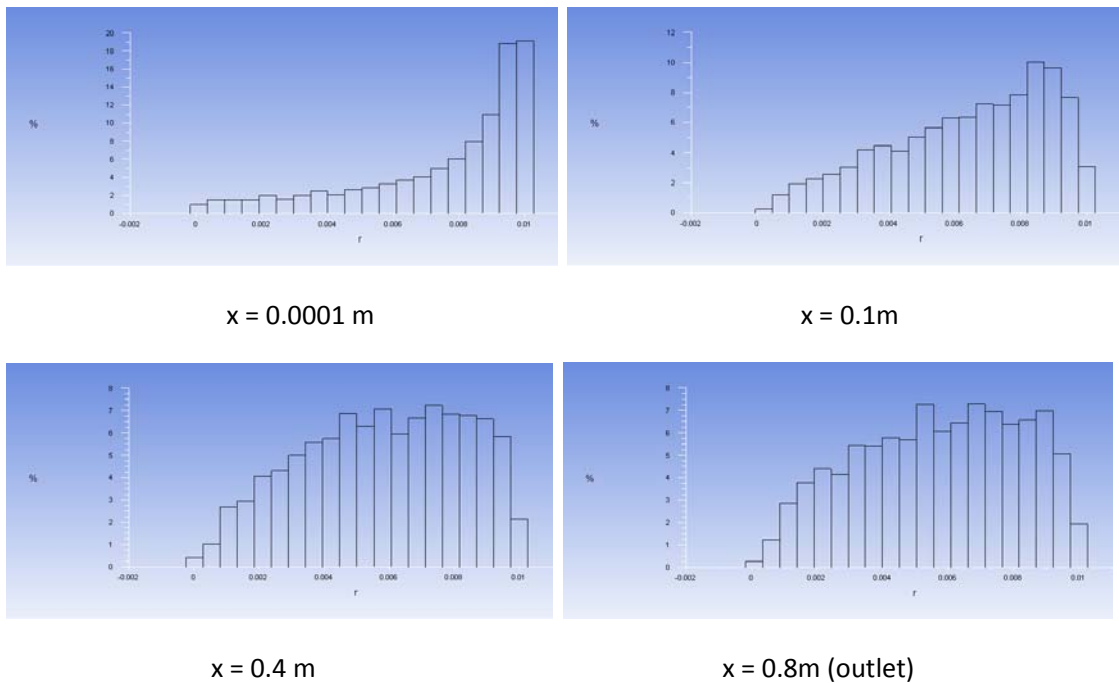


Figure 18. Histograms of Particle Locations at Various Cross Sections for Case 7

The above histograms show: at very near the inlet the particles are distributed by the scale of surface area, then as moving down stream, more particles tends to stay at the region of $0.0065\text{m} < r < 0.0095\text{m}$ ($0.65 < r/R < 0.95$).

It is also noted that particles are travelling back and forth in the pipe, so if there is thermal flux at the pipe wall, this behavior may help to improve the heat transfer from the wall to the fluid. Part of the particles trajectories are shown below in Figure 19:

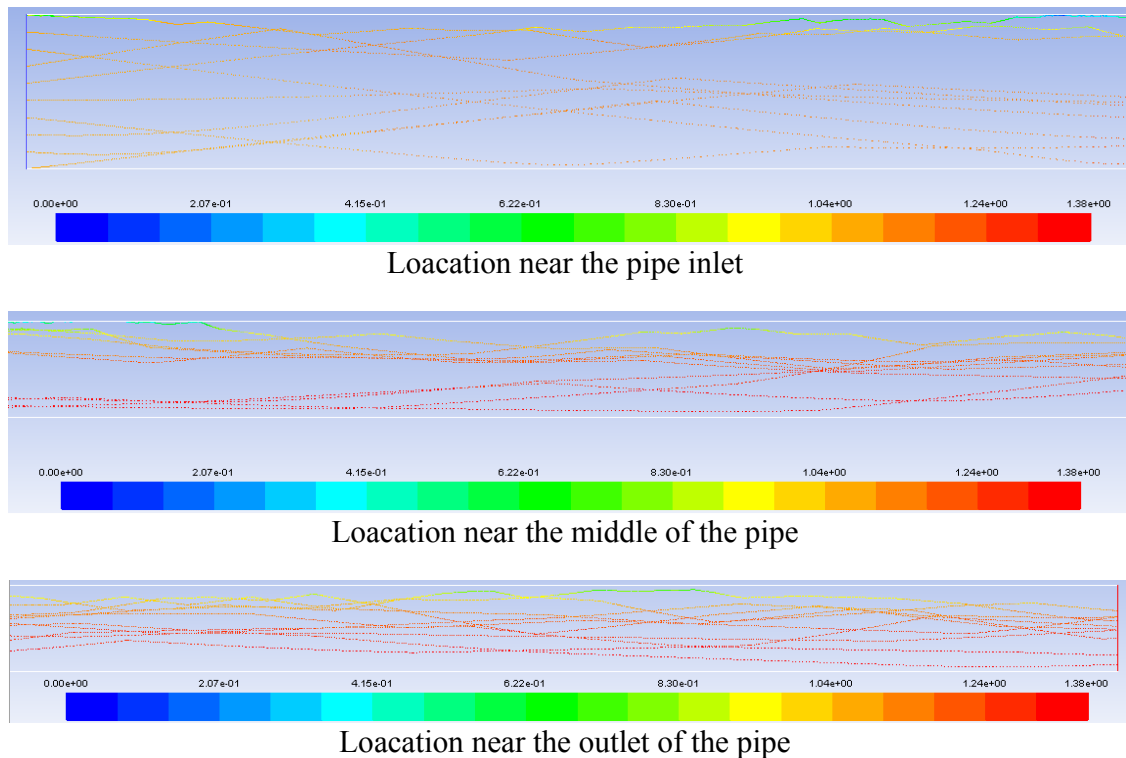


Figure 19. Particle Trajectories Colored by Particle Velocity

5.6.3. Particles Interact with Turbulence

Nanoparticles may interact with turbulence, Xuan and Li³² suggested that the presence of nanoparticles may lead to the intensification of turbulence or eddies. However, through a comparison of the nanoparticle and turbulent eddy time and length scales, Buongiorno³³ shows that the nanoparticles move homogeneously with the fluid in the presence of turbulent eddies, so an effect on turbulence intensity is doubtful.

The turbulence intensity at the outlet is examined, and the figure of turbulence intensity is plotted vs. the nondimensionalized radius r/R in Figure 20.

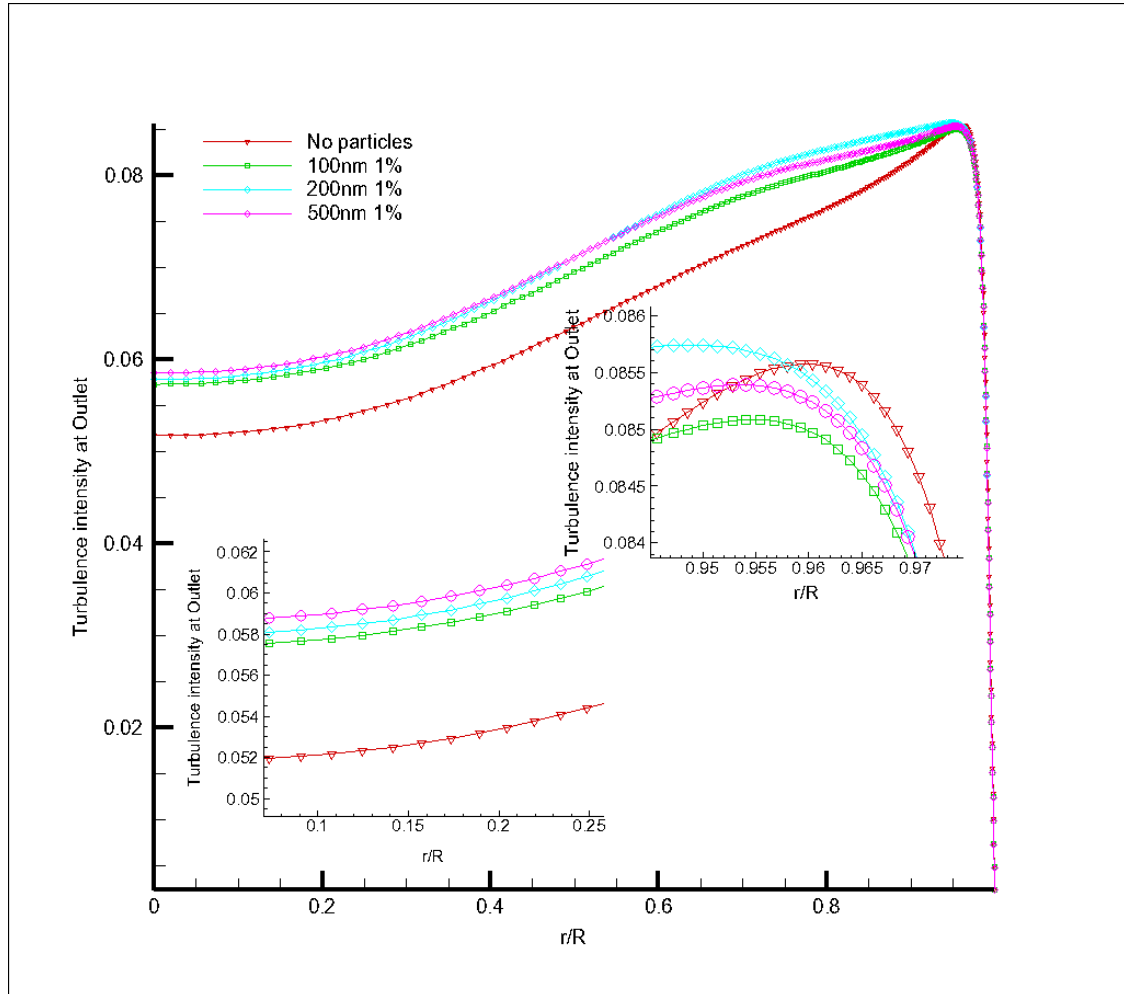


Figure 20. Turbulence Intensity vs r/R for 1% Particle Volume Fraction

The center line turbulence intensity for fully developed pipe flow can be estimated through the empirical correlation below:

$$I = 0.16 \left(\text{Re}_{D_H} \right)^{-\frac{1}{8}} \quad (50)$$

As in the present study with Reynolds number of 19,560, the correlation gives a resultant turbulence intensity of about 4.7%, while our simulation gives turbulence intensity as 5.1%. Compare with the correlation, the present result has an error about 9%.

The effect of nanoparticles on turbulence intensity is shown in Figure 20, the turbulence intensity increased in most of the region ($r/R < 0.95$) except at the near wall region ($r/R > 0.95$), the turbulence intensities for all the cases are close. From Figure 20, it is found that larger particle size may correspond to greater turbulence intensity. As a result, the increasing in turbulence intensity may aid in mixing the fluid and improve the heat transfer properties.

Figure 21, below is showing the turbulence dissipation rate at the outlet where $x = 0.8$ m.

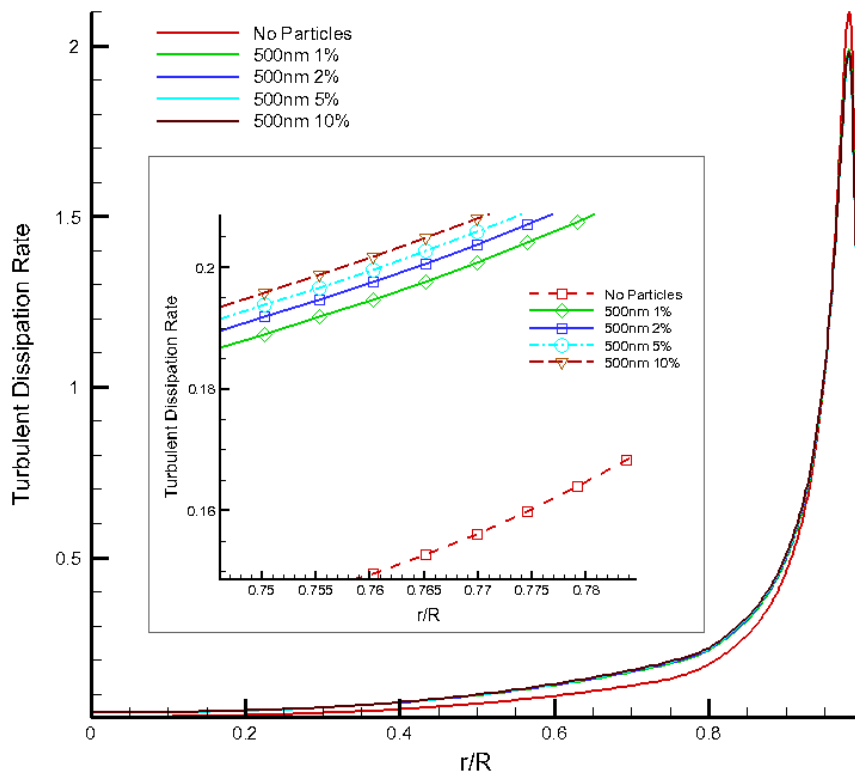


Figure 21. Turbulence Dissipation rate at Outlet vs Dimensionless Radius

It is noted that in the region between $0.2 < r/R < 0.9$ nanoparticle can accelerates the dissipation rate of turbulence kinetic energy, while in the near wall region the dissipation rate of nanofluids is less than that of pure fluid. The reason for the increase in dissipation rate may be that the particles can interact with the smallest eddies and gain energy from those small eddies, and hence the kinetic energy of the fluid will dissipate quickly. But, the particles can also interact with fluids and form wake downstream of the particles, this may increase the total fluid kinetic energy.

Chapter 6. Conclusions

Numerical simulations of fluid and nanoparticles two phase flow are conducted through using the finite volume method. In laminar flow modeling, flows with different inlet boundary conditions were studied and particle dynamics are discussed; Numerical simulations of turbulent flow containing nanoparticles of different size and load are conducted. Particle migration in both laminar and turbulent flow were studied, and their interaction with turbulence and eddies was discussed.

In laminar flow with plug inlet flow, nanoparticles are travel toward the center line and lead to a non-uniform particle concentration; On the other hand with the fully developed inlet boundary conditions at inlet, nanoparticles travel parallel with the pipe wall, and the original concentration will be conserved.

For turbulence pipe flow containing different particle size and load, the following conclusions are made:

1. The presence of nanoparticles lead to an increase of drag coefficient, the drag increment is proportional to the particle load, the maximum increment, which is 5%, is associated with the case of 10% volume concentration;
2. Particle dispersion in fully developed turbulent flow is not uniform, more particles are present in the region of $0.65 < r/R < 0.95$.
3. Particle trajectories shows particles tends to move back and forth in the middle of the pipe;
4. The presence of nano particles can lead to increase of turbulence intensity in the region far from the wall; and larger particle size corresponds to greater turbulence intensity;

5. In the region away from the wall where $0.2 < r/R < 0.85$, the dissipation rate of flow with nanoparticles is in average around 30% higher than that of single phase flow. High turbulence dissipation rate and high turbulence intensity is indicating the production of kinetic energy should be higher in the presence of nanoparticles.

Chapter 7. Future Research

Future research should employ unsteady tracking in the Lagrangian domain, or even do transient simulations in both the Eulerian and Lagrangian domain. This is because turbulence is time dependent and with transient simulation, the flow properties are considered as a function of time. Since turbulence and eddies are always three dimensional, the use of three dimensional (3D) simulation should be included. 2D RANS simulation can only roughly capture the behaviors of nanoparticles and the mean velocity of the fluids. Also a LES simulation is suggested, because this can give a view of how the particles act with the large eddies. Particle to particle interaction should also be included in the future research, especially in the high concentration case. That is because when the particle load is high, the particles may collide more frequently and the effect of particle collision should not be ignored. As a next step, the energy equation should be considered, in order to investigate the heat transfer property of nanofluids and its relation to particle migration, this may help to build the next generation of coolants.

BIBLIOGRAPHY

- [1] J. C. Maxwell, A Treatise on Electricity and Magnetism, 3rd ed. (Dover, New York, 1954), Vol. 1, p. 435.
- [2] R. L. Hamilton and O. K. Crosser, Thermal conductivity of heterogeneous two-component systems, *Ind. Eng. Chem. Fundam.* 1, 187(1962).
- [3] S. U. S. Choi, Developments and Applications of Non-Newtonian Flows, (ASME, New York, 1995), FED-Vol. 231, p. 99.
- [4] S. Choi, etc. Enhancing Thermal Conductivity of Fluids with Nanoparticles. 1995 International mechanical engineering congress and exhibition, San Francisco, CA (United States), 12-17 Nov 1995; Other Information: PBD: Oct 1995
- [5] S. Choi, etc. Anomalous Thermal Conductivity Enhancements in Nanotube Suspensions. *Applied Physical Letters* 79.14 (2001): 2252-2254.
- [6] H.Chen, W,Yang etc, Heat transfer and flow behaviour of aqueous suspensions of titanate nanotubes (nanofluids), *Powder Technology* 2008
- [7] H. U. Kang, S. H. Kim, & J. M. Oh, Estimation of Thermal Conductivity of Nanofluid Using Experimental Effective Particle Volume, *Exp. Heat Transfer* 19, 181, 2006.
- [8] M. Chopkar, P. K. Das, and I. Manna, Synthesis and characterization of nanofluid for advanced heat transfer applications, *Scr. Mater.* 55, 549 (2006).
- [9] J. Philip, P. D. Shima and R. Baldev, Evidence for enhanced thermal conduction through percolating structures in nanofluids, *Nanotechnology* 19, 305706 (2008).
- [10] H. E. Patel, T. Sundararajan, and S. K. Das, A cell model approach for thermal conductivity of nanofluids, *J. Nanopart. Res.* 10, 87 (2008).

- [11] J. Eapen, J. Li, and S. Yip, Mechanism of Thermal Transport in Dilute Nanocolloids, *Phys. Rev. Lett.* 98, 028302 (2007).
- [12] J. Buongiorno et al, A benchmark study on thermal conductivity on nanofluids, *Journal of Applied Physics* 106, 094312, 2009
- [13] C. W. Nan, R. Birringer, D. R. Clarke, and H. Gleiter, Effective thermal conductivity of particulate composites with interfacial thermal resistance, *J. Appl. Phys.* 81, 6692 (1997).
- [14] Yulong Ding, Dongsheng Wen, Particle migration in a flow of nanoparticle suspensions, *Powder Technology*, Volume 149, Issues 2-3, 3 January 2005, Pages 84-92, ISSN 0032-5910, DOI: 10.1016/j.powtec.2004.11.012.
- [15] M Giraldo, Y Ding and R A Williams, Boundary integral study of nanoparticle flow behaviour in the proximity of a solid wall, 2008 *J. Phys. D: Appl. Phys.* 41 085503 doi: 10.1088/0022-3727/41/8/085503
- [16] Batchelor, G. *Introduction to Fluid Mechanics*, Cambridge University Press (2000)
- [17] C. M. Rhie and W. L. Chow. Numerical Study of the Turbulent Flow Past an Airfoil with Trailing Edge Separation. *AIAA Journal*, 21(11):1525–1532, November 1983.
- [18] ANSYS® FLUENT® 12.0 Theory Guide, Release 12.0 © ANSYS, Inc. 2009-01-29
- [19] Robert W. Fox, Philip J. Pritchard, Alan T. McDonald, *Introduction to Fluid Mechanics*, 7th Edition, ISBN 978-0-470-45927-0, August 2008, ©2009
- [10] J. R. Cash and A. H. Karp, A variable order Runge-Kutta method for initial value problems with rapidly varying right-hand sides. *ACM Transactions on Mathematical Software*, 16:201-222, 1990.
- [21] S. A. Morsi and A. J. Alexander. An Investigation of Particle Trajectories in Two-Phase Flow Systems. *J. Fluid Mech.*, 55(2):193-208, September 26 1972.

- [22] H. Ounis, G. Ahmadi, and J. B. McLaughlin. Brownian Diffusion of Submicrometer Particles in the Viscous Sublayer. *Journal of Colloid and Interface Science*, 143(1):266–277, 1991.
- [23] Serway, Raymond, *Physics for Scientists and Engineers with Modern Physics*, 3rdEd, Saunders College Publishing, (1990)
- [24] Li A and Ahmadi G, 1993, Deposition of aerosols on surfaces in a turbulent channel flow, *Int. J. Eng. Sci.* 31 435–51
- [25] Y.C. Lam, X. Chen, K.W. Tan, J.C. Chai, S.C.M. Yu, Numerical investigation of particle migration in Poiseuille flow of composite system, *Composites Sci. and Technol.* 64 (2004) 1001– 1010.
- [26] P. G. Saffman. The Lift on a Small Sphere in a Slow Shear Flow. *J. Fluid Mech.*, 22:385-400, 1965.
- [27] A. Li and G. Ahmadi. Dispersion and Deposition of Spherical Particles from Point Sources in a Turbulent Channel Flow. *Aerosol Science and Technology*, 16:209-226, 1992.
- [28] J. O. Hinze. *Turbulence*. McGraw-Hill Publishing Co., New York, 1975.
- [29] B. E. Launder and D. B. Spalding. *Lectures in Mathematical Models of Turbulence*. Academic Press, London, England, 1972.
- [30] T.-H. Shih, W. W. Liou, A. Shabbir, Z. Yang, and J. Zhu. "A New - Eddy-Viscosity Model for High Reynolds Number Turbulent Flows - Model Development and Validation". *Computers Fluids*. 24(3). 227–238. 1995.
- [31] Pearson, K. (1905). The problem of the Random Walk. *Nature*. 72, 294.
- [32] Xuan, Y., and Li, Q., 2003, "Investigation on Convective Heat Transfer and Flow Features of Nanofluids," *J. Heat Transfer*, 125, pp. 151–155.

[33] J. Buongiorno, Convective Transport in Nanofluids, J. Heat Transfer , March 2006,
Volume 128, Issue 3, 240

Vita

Kai Jin the son of Wenzhi Jin and Yunxiang Xue was born in Taiyuan, China on Aug. 5, 1986. His preliminary education was in his home town. He earned his Bachelor's Degree in Mechanical Engineering from Shandong University of Technology, China, 2009. Afterwards he went to Lehigh University, USA to pursue his Master of Science degree in Mechanical Engineering. Kai is also participating in the Lehigh University's Industrial Assessment Center program. He is currently submitting this thesis for the M.S. degree in Mechanical Engineering.